# Influence of Morpho-Structural Parameters on Environmental Stress Cracking in Polyethylene

*F. Olla[1*], M. Contino[1], D. Ferri[2], F. Scavello[2], L. Andena[1]*

*[1]Dipartimento di Chimica, Materiali e Ingegneria Chimica "Giulio Natta", Politecnico di Milano, Piazza Leonardo da Vinci, 32, 20133, Milano (MI), Italy*

*[2]Versalis S.p.A., Mantua Research Center, Via G. Taliercio 14, 46100 Mantova, Italy.*

** Corresponding author.*
*E-mail address: federico.olla@polimi.it (F. Olla)*

**Abstract**

Polyethylene (PE) is widely utilized in several industries due to its versatility and mechanical strength, yet its long-term performance is often hindered by slow crack growth (SCG) and environmental stress cracking (ESC). This study quantitatively evaluates the influence of key morpho-structural parameters on SCG and ESC resistance in PE, using a linear elastic fracture mechanics (LEFM) approach to assess the effect of different comonomers on fracture toughness. Four PE materials were analyzed: two medium molecular weight, linear low-density polyethylenes (LLDPE) co-polymerized with 1-butene (Material A) and 1-hexene (Material B); a high molecular weight LLDPE copolymerized with 1-hexene (Material C); and a medium molecular weight, high-density polyethylene (HDPE) homopolymer (Material D). The results confirm that molecular weight is a dominant factor in enhancing stress cracking resistance, with the high molecular weight LLDPE (Material C) showing superior performance. Moreover, despite nearly identical structural parameters, Material B exhibited significantly higher SCG and ESC resistance compared to Material A, highlighting the critical role of the commoner type. The research identified three distinct environmental regimes influencing fracture behavior, each dependent on the applied stress intensity factor ($K$) and material properties. These regimes are: (1) no significant environmental effect at high $K$ values, where fracture is dominated by the material's inherent properties; (2) partial plasticization of craze fibrils at intermediate $K$ values, due to limited diffusion of environmental agents into the crack tip; and (3) full plasticization of craze fibrils at low $K$ values, where extensive diffusion accelerates environmental stress cracking (ESC). By demonstrating how morpho-structural parameters and environmental conditions together influence polyethylene's resistance to SCG and ESC, this study improves our understanding of the underlying mechanisms and underscores the effectiveness of LEFM in evaluating long-term material performance. This knowledge can guide the design with polyethylene materials aimed at improving long-term durability for industrial applications.

**Keywords**

Polyethylene; comonomer; fracture mechanics; slow crack growth; environmental stress cracking.

**Nomenclature**

| | |
|---|---|
| $PE$ | Polyethylene |
| $SCG$ | Slow Crack Growth |
| $ESC$ | Environmental Stress Cracking |
| $ESCR$ | Environmental Stress Cracking Resistance |
| $HDPE$ | High Density Polyethylene |
| $LLDPE$ | Linear Low-Density Polyethylene |
| $TM$ | Tie Molecule |
| $a$ | Crack length |
| $a_0$ | Initial crack length |
| $a_f$ | Final crack length |
| $t$ | Time |
| $t_i$ | Initiation time |
| $t_p$ | Propagation time |
| $t_f$ | Total time to failure |
| $K$ | Mode I stress intensity factor |
| $G$ | Mode I energy release rate |
| $A_1$ | Constant material dependent value relating crack initiation to the stress intensity factor $K$ |
| $n$ | Constant material dependent value relating crack initiation to the stress intensity factor $K$ |
| $A_2$ | Constant material dependent value relating crack speed to the stress intensity factor $K$ |
| $m$ | Constant material dependent value relating crack speed to the stress intensity factor $K$ |
| $M$ | Molecular weight |
| $P(M)$ | Probability of formation of a Tie Molecule for a linear chain of molecular weight M |
| $r$ | End-to-end distance of an ideal chain |
| $< r^2 >$ | Mean square value of the end-to-end distance |
| $b$ | Coefficient of the H-B model defined as $b^2 = \frac{3}{2<r^2>}$ |
| $n(M)$ | Number of molecules with a molecular weight between $M$ and $M + dM$ |
| $P_{TM}$ | Probability of formation of a tie molecule for a given molecular weight distribution, it represents the fraction of molecules that form tie molecules |
| $l_c$ | Lamella thickness |
| $l_a$ | Amorphous phase thickness |
| $L_p$ | Long period, defined as $L_p = 2l_c + l_a$ |
| $R_g$ | Radius of gyration |

| | |
|---|---|
| $M_n$ | Number-average molecular weight |
| $M_w$ | Weight-average molecular weight |
| $MWD$ | Molecular weight distribution |
| H-B | Huang-Brown model |
| $SCB$ | Short Chain Branching |
| $SCBD$ | Short Chain Branching Distribution |
| $GPC$ | Gel Permeation Chromatography |
| $NMR$ | Nuclear Magnetic Resonance |
| $DSC$ | Differential Scanning Calorimetry |
| $CM$ | Compression Moulded |
| $FPB$ | Four Point Bending |
| $\sigma$ | Stress |
| $\varepsilon$ | Strain |
| $E(t)$ | Time-dependent relaxation modulus |
| $F50$ | Time taken for 50% of the Bell Telephone Test specimens to fail |
| $SENB$ | Single Edge Notched Bending |
| $W$ | SENB specimen Width |
| $B$ | SENB specimen thickness |
| $B_g$ | SENB specimen grooved thickness |
| $L$ | Span length in FPB configuration |
| $LVDT$ | Linear Variable Displacement Transducer |
| $P$ | Applied load |
| $Y\left(\frac{a}{W}\right)$ | Shape factor to calculate the stress intensity factor |
| $B^*$ | Effective thickness of grooved SENB samples |
| $u$ | Displacement |
| $\psi\left(\frac{a}{W}\right)$ | Energy release rate calibration factor |
| $\psi_{FPB}\left(\frac{a}{W}\right)$ | Energy release rate calibration factor relative to Four Point Bending configuration |
| $\nu$ | Poisson's ratio |
| $\sigma_{true}$ | True stress |
| $\lambda$ | Stretch |
| $< G_p >$ | Strain hardening modulus |

| | |
|---|---|
| $Q$ | Flow rate |
| $k$ | Permeability |
| $\eta$ | Viscosity |
| $\nabla p$ | Pressure gradient |
| C | Sample compliance |
| $D(t)$ | Time dependent creep compliance |
| $C(0)$ | Initial compliance of a specimen without any defect |
| $\Delta_{FPB}$ | The deflection of a beam in a four-point bending (FPB) setup |
| $\phi\left(\frac{a}{W}\right)$ | Geometric factor in the compliance calibration equation |
| $D^*(t)$ | Apparent compliance |

## 1. Introduction

Polyethylene (PE) is one of the most widely produced plastics globally due to its versatility, durability, and cost-effectiveness. The polymer's widespread use is due to its excellent chemical resistance, good mechanical properties, and ease of processing, making it a staple material in numerous industries.

From an engineering standpoint, to design long-lasting polyethylene products, three primary failure modes must be considered: ductile failure, quasi-brittle failure, also known as rapid crack propagation (RCP), and brittle failure known as slow crack growth (SCG) [1].

Ductile failure occurs when the material undergoes significant plastic deformation before rupture. The controlling factor for this failure is the yield stress of the polymer. In standard tests on pipes at constant hydrostatic pressure [2] it is typically associated with localized expansion or "ballooning" of the pipe [1,3,4].

Rapid crack propagation (RCP) occurs when a component is subjected to a sudden and intense load, usually at low temperatures. In this failure mode, any pre-existing or newly initiated crack can propagate through the material at extremely high speeds, often exceeding 100 m/s. Unlike ductile failure, RCP happens with minimal or no plastic deformation and can result in catastrophic failure [5,6].

Slow crack growth (SCG) is usually the most dominant failure mechanism in polyethylene products, typically occurring over extended periods under sustained low-stress conditions. It is typically initiated by surface imperfections such as scratches or notches, which act as stress concentrators, causing crack formation and propagation [7–9]. SCG develops slowly and often goes unnoticed until the material reaches a critical point, leading to failure. SCG can be driven by intrinsic properties of the material or accelerated by the influence of the environment. This phenomenon is particularly critical in applications requiring long-term durability, such as gas pipes, water distribution systems, and storage tanks.

A phenomenon closely related to SCG is Environmental Stress Cracking (ESC), in which the progression of slow crack growth is accelerated when polyethylene is exposed to surface-active agents under stress. These agents do not alter the polymer's chemical structure but drastically reduce the time to failure, by accelerating crack initiation and propagation. ESC often begins with localized crazing and cracking, triggered by the plasticization of the polymer surface in contact with environmental factors like chemicals or solvents. In ESC, the same crack growth mechanisms observed in SCG occur, but at a significantly accelerated rate due to environmental factors, making it a critical consideration in the design of polyethylene products intended for long-term use

under stress [10,11]. Over the past four decades, the practical importance of slow crack growth has driven the polyethylene industry to continuously develop improved resins with enhanced SCG resistance [6,12–14]. As a result, SCG remains a key area of research due to its ongoing relevance in ensuring the long-term durability of PE products in demanding applications [1,15–19]. Additionally, since active environments in ESC accelerate the same crack growth mechanisms of SCG, this phenomenon is exploited to expedite the testing of increasingly tough materials, providing valuable predictive insights into their long-term performance in a reduced amount of time.

The resistance of polyethylene to SCG and ESC is closely tied to its molecular structure, with its behavior under stress determined by several key morpho-structural parameters playing a critical role in its behavior under stress [12,21]. This article aims to quantitatively evaluate the influence of these parameters using a linear elastic fracture mechanics (LEFM) approach, particularly focusing on how different types of comonomer affect fracture toughness. By applying LEFM, a clearer understanding of the mechanisms through which comonomers modify the material's resistance to slow crack growth can be established, ultimately offering insights into optimizing the long-term performance of polyethylene under various stress conditions. Traditional testing methods for assessing stress cracking often provide qualitative or comparative data that can be influenced by testing conditions and material properties unrelated to fracture resistance, such as sample geometry or environmental factors. Moreover, their limitations, in terms of both the amount of information provided (typically a single ranking parameter) and its accuracy, hinder the possibility of establishing clear structure-properties relationships for the materials under investigation. The application of LEFM is thus crucial to achieve the objectives of this study. Additionally, a LEFM-based approach can provide reliable quantitative predictions of product lifetime, which can be of high interest for the industry (e.g. in view of optimizing the content of recycled materials, striking an optimal balance between performance and sustainability).

## 2. Background

### 2.1 SCG and ESC testing methods

Accurately assessing slow crack growth resistance in polyethylene is essential for predicting the long-term performance of PE products. To address this need, various testing methods have been developed, spanning from conventional long-term tests to accelerated techniques leveraging ESC mechanisms, such as the Full Notch Creep Test [20], Pennsylvania Edge Notched Tensile test [21] and Cracked Round Bar [13,22–28]. The following section outlines the specific methods employed in this study.

- Bell Telephone Test: the Bell Telephone test [29] is a well-established method used to evaluate the ESC resistance of ethylene plastics. Bent specimens, each containing a controlled defect, are exposed to surface-active agents under a constant strain and temperature. The test measures the time until cracking occurs. It is one of the oldest SCG testing methods and it has been selected because it is the current standard adopted at the industrial level to evaluate the Environmental Stress Cracking Resistance (ESCR) of polyethylene materials.
- Strain Hardening Modulus Test (SHM): In recent years, the strain hardening modulus has gained widespread recognition as a reliable and efficient method to evaluate SCG behavior in polyethylene materials [19,30–33] and it has become a standard measure to predict resistance to stress cracking [34]. Derived from a simple tensile test performed at high temperature, this parameter provides a faster alternative to traditional long-term SCG tests and is increasingly being adopted within the industry. A high strain hardening modulus is expected to reflect a high resistance to disentanglement of the tie molecules within the polymer structure, factor that should also govern resistance to SCG [30]. The SHM Test is particularly attractive for ranking purposes due to its straightforward specimen

preparation and ease of execution; the main difficulty associated with the method is the need for a sufficiently large crosshead stroke, which could be limited by the oven size.

- Fracture Mechanics (FM): Fracture Mechanics represents the state of the art of fracture testing and can provide predictive information, leading to a richer material characterization. In particular, if the size of the plastic zone near the crack tip is negligible Linear Elastic Fracture Mechanics (LEFM) principles can be adopted [35–37]. Although a standardized method for testing SCG and ESC with LEFM does not currently exist, this framework has been successfully employed to quantitatively predict the phenomenon in polymers [9,17,38–48]. Due to the intrinsic viscoelastic nature of polymers, the time-dependent aspect of fracture behavior must also be considered. In fact, to study the time dependency of fracture in viscoelastic materials, the total failure time $t_f$ should be calculated as:

$$t_f = t_i + t_p \quad (1)$$

where $t_i$ is the crack initiation time and $t_p$ is the propagation time needed for the crack to grow until failure. These characteristic times depend on the properties of the material through the stress intensity factor $K$; in the present work only mode I is considered. Power law dependencies such as those reported in Equations 2 and 3 are usually chosen to represent the fracture behaviour of polymers [36,49]:

$$t_i = A_1 \cdot K^n \quad (2)$$

$$\frac{da}{dt} = A_2 \cdot K^m \quad (3)$$

where $A_1$, $A_2$, $n$ and $m$ are constant values related to the properties of the material and the considered environment. Knowing the initial crack length $a_0$ and the failure crack length $a_f$, it is hence possible to determine the propagation time by simple integration:

$$t_p = \int_{a_0}^{a_f} \frac{da}{A_2 \cdot K^m} \quad (4)$$

Finally, by combining Equations 1, 2 and 4 and knowing the value of the applied mechanical stress (related to $K$), it will be possible to predict the lifetime of a given component.

### 2.2 Tie Molecules in Polyethylene SCG

SCG generally occurs when a tensile load induces high stress concentrations at specific sites within the polymer, such as those formed by scratches, flaws, cracks, dust particles, or molecular heterogeneities [32,35]. These stress concentrations induce yielding in the amorphous regions, followed by the fragmentation of crystalline lamellae and partial chain unfolding [25,50]. This sequence of events leads to the formation of crazes in localized regions where highly oriented microfibrils bridge the gap across the developing crack. Although these crazes temporarily resist crack propagation, the fibrils eventually fail under continued stress [51–53]. Fracture under SCG conditions is generally interlamellar, meaning it occurs between the crystalline lamellae, as has been observed in the literature [54,55]. The interlamellar nature of SCG is crucial because tie molecules play a fundamental role in connecting adjacent crystalline regions through the amorphous phase [56]. These tie molecules, which bridge the lamellae, are widely regarded as the primary mechanism for resisting fracture [57–59]. When stress is applied, tie molecules stretch and absorb energy, preventing the lamellae from separating. However, under prolonged stress, particularly at low stress levels, these tie

molecules gradually untangle and break, leading to the brittle failure of the material [60,61].
The density of tie molecules is a critical factor in determining polyethylene's resistance to SCG, since it is directly related to the mechanical resistance of craze fibrils [7,62].

The number of the tie molecules and their effectiveness in resisting fracture strongly depend on the molecular structure. The Huang-Brown (H-B) model [58,63], one of the earliest proposed frameworks, provides a simple yet effective approach to understand how molecular weight, crystallinity, and chain architecture impact tie molecule formation. While later models have expanded and refined this approach [59,64–69], the H-B model remains a valuable tool in describing how these molecular parameters affect SCG. According to the model, tie molecules can form when polymer chains are long enough to span the amorphous layer and connect adjacent lamellae (Figure 1). The probability of a chain forming a tie molecule is governed by its molecular weight and the thickness of the crystalline and amorphous layers.

Assuming that the chain topology is generally preserved after crystallization [70], the probability of formation of a Tie Molecule (TM) for a linear chain of molecular weight *M* is:

$$P(M) = \frac{1}{3}\frac{\int_{L_p}^{\infty} r^2 \exp(-b^2 r^2)\, dr}{\int_0^{\infty} r^2 \exp(-b^2 r^2)\, dr} \qquad (5)$$

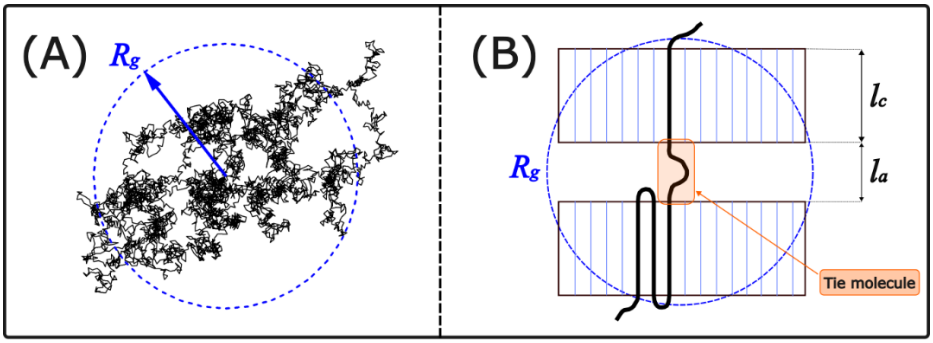


***Figure 1:*** ***(A)*** *Random coil configuration of an ideal chain of PE showing the corresponding radius of gyration ($R_g$).* ***(B)*** *Illustration of the conditions required to form tie molecules, as defined by Huang and Brown [58,63].*

Where $b^2 = \frac{3}{2<r^2>}$ and $< r^2 >$ is the mean square value of the end-to-end distance, which is proportional to *M*. The value of $P$ gives the probability for a randomly coiled chain of a particular molecular length to span a distance $L_p = 2l_c + l_a$, where $l_c$ is the lamella thickness and $l_a$is the amorphous phase thickness. The factor $\frac{1}{3}$ was introduced because two dimensions of the lamellar structure are much larger than the long period $L_p$.

Equation 5 is valid for an ideal monodisperse system. For a real polymer the actual distribution of molecular weights must be taken into account; therefore, the probability of formation of a tie molecule for a given molecular weight distribution is:

$$P_{TM} = \frac{\int_0^{\infty} n(M)P(M)dM}{\int_0^{\infty} n(M)dM} \qquad (6)$$

where $n(M)$ is the number of molecules with a molecular weight between $M$ and $M + dM$. Following this approach, the probability $P_{TM}$ represents the fraction of molecules that form tie molecules [58].

While experimental techniques for measuring the density of tie molecules have been developed [64,71–74], they often require sophisticated equipment or are time-consuming, which can limit their widespread use. In contrast, the H-B model offers a simpler and more accessible approach to estimate TM concentration.

However, the model has its limitations: it doesn't account for complex features such as chain entanglements and branching, and it only considers two-lamella connections, which fails to capture the behavior of longer molecules that can form multi-lamellar networks. Although not a comprehensive model of the SCG process, the H-B framework remains a valuable tool for gaining insights into how structural parameters such as molecular weight, short chain branching, and crystallinity may influence SCG resistance.

### 2.3 Structural parameters that affect SCG and ESC resistance

The resistance of polyethylene to SCG and ESC is closely tied to its molecular structure, with its behavior under stress determined by several key morpho-structural parameters [12,75]. Below, the most relevant parameters which influence fracture toughness are presented, listed according to their relative importance with respect to stress cracking behavior.

Molecular weight: Molecular weight is a crucial factor in determining polyethylene's resistance to SCG and ESC. Since the 1950s [8], it has been observed that higher molecular weight grades of polyethylene exhibit significantly better resistance to these failure mechanisms. This improvement is primarily due to the increased formation of tie molecules. Today, the relationship between molecular weight and tie molecule density is accepted as one of the key determinants of fracture toughness in polyethylene [12,58,75–77]. However, increasing molecular weight presents challenges in terms of processability. Higher molecular weight polymers have increased viscosity, which can hinder manufacturing processes.

Degree of crystallinity and crystallite dimensions: The degree of crystallinity in polyethylene plays a key role in its resistance to SCG and ESC, with lamellar thickness being the primary contributor to this influence. Crystalline regions provide the material's rigidity and increase resistance to ductile failure, but thicker lamellae reduce the number of tie molecules leading to a trade-off between stiffness and toughness. Lu and Brown [78] demonstrated that faster cooling produces thinner lamellae, which may reduce the material's stiffness but enhance its resistance to ESC, while slower cooling promotes the formation of thicker lamellae. To optimize polyethylene's resistance to stress cracking, lamellar thickness must be carefully managed. A balance between sufficiently thick lamellae to provide structural integrity and enough tie molecules to maintain toughness is essential. For the same molecular weight, the H-B model predicts a higher probability of forming a tie molecule for a system with thinner lamellae (see Figure 2). However, drawing definitive conclusions remains challenging, as the thickness of both the amorphous phase and the crystalline lamellae also depends on molecular weight [79].

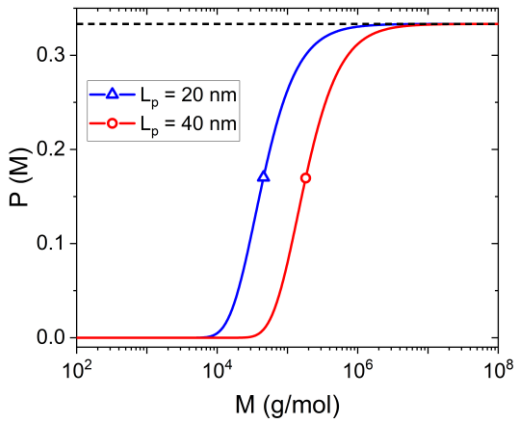


***Figure 2**: Probability of forming a tie molecule (P(M)) as a function of molecular weight (M) for a monodisperse system, calculated using the Huang-Brown (H-B) model. The calculations are made for long periods $L_p=2l_c+l_a$ of 20 nm and 40 nm. The dashed line represents the maximum probability of 1/3 for tie molecule formation.*

Short chain branching: Short chain branching (SCB) is another critical factor that influences the mechanical properties of polyethylene (PE). The effect of SCB on PE is primarily mediated through its impact on crystallinity and the polymer's microstructure. Short chain branches disrupt crystallinity, making the polymer

more flexible and increasing the density of tie molecules for the same molecular weight [80,81]. The presence of short chain branches, such as butyl groups, significantly slows the crack growth rate compared to homopolymers. A copolymer can exhibit a SCG rate several orders of magnitude slower than a homopolymer with comparable molecular weight and density. This slower crack propagation is also attributed to the increased difficulty of disentangling branched molecules through the crystalline regions, making it harder for cracks to propagate (Figure 3) [63,82].

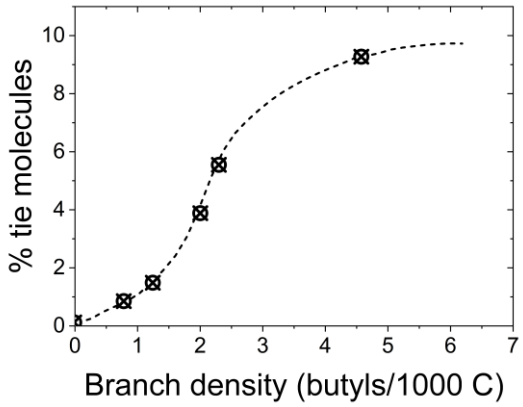


***Figure 3:*** *Percentage fraction of tie molecules plotted against butyl branch density, adapted from [63].*

Short chain branching distribution: The distribution of short chain branches (SCBD) significantly affects the crystallization behavior, mechanical properties, and long-term fracture resistance of polyethylene. Including short chain branches within high molecular weight chains promotes the formation of tie molecules [83–85]. In multimodal PE resins, the preferential placement of SCBs in the high molecular weight fraction significantly enhances ESC resistance and other long-term mechanical properties [6,64]. Heterogeneities in branch distribution can also alter the initiation and propagation of cracks under stress [15]. Thus, optimizing SCBD in PE resins is essential for applications requiring long-term durability.

Molecular weight distribution: The molecular weight distribution (MWD) is another key factor influencing SCG and ESC resistance in polyethylene. In monodisperse systems, there is limited experimental evidence directly linking MWD to SCG and ESC resistance. Hosoda et al. [86] conducted detailed investigations on fractionated linear low-density polyethylene (LLDPE), showing that MWD affects the formation of tie molecules. They found that molecular weight fractions above $5 \cdot 10^4$ g/mol contribute notably to the material toughness, increasing the concentration of tie molecules, while the lower molecular weights behave in a very brittle manner. Materials with higher molecular weight fractions are more likely to form the tie molecules necessary for resisting long-term stress cracking. Despite the experimental gaps in understanding the role of MWD in SCG and ESC for monodisperse systems, the H-B model can be used to examine the probability of tie molecule formation for a gaussian molecular weight distribution system. As the attached graph illustrates (Figure 4), the results indicate that the number-average molecular weight ($M_n$) exerts minimal influence on tie molecule density, with the weight-average molecular weight ($M_w$) being the primary factor determining tie molecule formation. This suggests that, within monodisperse systems, MWD plays a limited role, and fracture resistance is predominantly governed by $M_w$. It is important to note that the H-B model does not account for the possibility of longer chains forming multiple connections between lamellae, potentially underestimating the contribution of high molecular weight molecules.

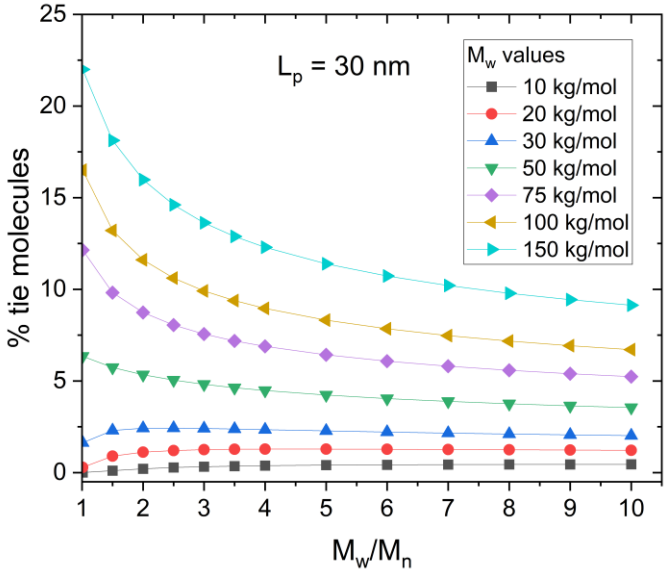


***Figure 4:*** *The predicted percentage of tie molecules is presented as a function of the polydispersity index ($M_w/M_n$) for polyethylene systems with varying weight-average molecular weights. These calculations are based on the Huang-Brown model, assuming a constant long period ($L_p$) of 30 nm and considering the molecular weight distribution curve to follow a Gaussian profile.*

In contrast, bimodal and multimodal polyethylene systems exhibit a much more significant influence of MWD on SCG and ESC resistance. Bimodal resins enable the incorporation of SCB predominantly on the longer polymer chains within the MWD, enhancing the formation of tie molecules. The development of such materials has led to the creation of high-performance polyethylene grades, such as PE100, which combine high stiffness with superior crack resistance [6]. Multimodal systems, provide even greater control over mechanical properties and they also offer advantages in terms of processing, as they exhibit superior melt strength and are less prone to sagging during large-diameter pipe extrusion [6]. In summary, while the impact of MWD on SCG and ESC resistance in monodisperse systems appears limited, bimodal and multimodal systems leverage MWD to achieve superior mechanical properties.

Length of chain branch – type of comonomer: The impact of chain branch length on SCG resistance of PE is a complex and nuanced subject that remains an open question in the field. Literature suggests that the length of SCBs, such as ethyl, butyl, and hexyl groups, affects both crystallinity and tie molecule formation, thereby influencing SCG behavior. However, isolating the effect of branch length from other variables like molecular weight, branch content, and distribution is challenging. Gupta et al. [87] investigated this effect in linear low-density polyethylene (LLDPE) films and observed that longer branches significantly enhance crack propagation resistance. Similarly, Yeh et al. [88,89] found that increasing the length of SCBs improves static fatigue performance, with failure times rising considerably as branch length extends from ethyl to hexyl. They attributed this improved SCG resistance to the increased sliding resistance of longer SCBs, which makes it harder for polymer chains to disentangle and deform under stress. However, the precise mechanisms by which side chain length alters the microstructure, and thus influences fracture toughness, are not yet fully understood. For instance, Hosoda [90] conducted experimental measurements using C13 NMR and found that the probability of branch inclusion into the crystalline phase for both 1-butene and 1-hexene branches was similarly low, around 6%. This suggests minimal difference in their behavior during crystallization and indicates that both types of branches are predominantly excluded from the crystalline regions. Doran [91], using molecular dynamics simulations, reported that shorter branches like 1-butene are more likely to be incorporated into the crystalline phase than longer branches like 1-hexene. Specifically, the inclusion probability was 9.8% for 1-butene compared to just 2.5% for 1-hexene. This implies that shorter branches disrupt the crystalline lattice less, potentially affecting the material's mechanical properties differently than longer branches. Zhang [92] and Sanmartín [93] also contributed to this discussion through molecular dynamics simulations. Zhang found that both 1-butene and 1-hexene branches tend to be excluded from the

crystalline phase, decreasing crystallinity. Sanmartín observed that both butyl and hexyl branches are nearly completely excluded from crystalline regions, with the exclusion being slightly more pronounced for hexyl branches. These conflicting findings highlight the complexity of determining the exact role of branch length in SCG resistance. The discrepancies may arise from differences in methodologies, such as experimental measurements versus simulations, or from the difficulty in isolating the effect of branch length from other influencing factors like branch content and distribution, molecular weight, and crystallization conditions.

## 3. Materials

The project carried out during this research stems from a previous study conducted in 2020 [94]. The preliminary findings of the research laid the foundation for the current investigation. The polyethylene materials used in this study were kindly provided by Versalis, an industrial partner involved in this research. The materials were supplied as part of a collaborative effort to investigate the relationship between molecular structure and environmental stress cracking resistance. The focus of this work is on discerning the resistance to ESC of four distinct materials, three copolymers and one homopolymer:

(A) LLDPE 1-butene - medium $M_w$

(B) LLDPE 1-hexene - medium $M_w$

(C) LLDPE 1-hexene - high $M_w$

(D) HDPE Homopolymer - medium $M_w$

These materials were chosen based on their different expected resistance to ESC. Structural characterizations were carried out to highlight the factors influencing the presence of tie molecules in the polymers. The choice of this particular set of polyethylenes reflects a balance of factors known from the previous literature review and the existing know-how and capabilities of the material supplier. The comparison of materials A and B, which are almost identical except for their comonomer type, is a particularly exciting aspect of this research. Such a little variation provides a unique chance to investigate the effects of comonomer type on the material's Environmental Stress Cracking Resistance (ESCR).

The main molecular properties of interest that were analyzed are shown in Table 1. Precise values for certain properties are omitted for confidentiality reasons, and only the relative range is given.

***Table 1**: Properties of polyethylene materials A, B, C, and D. Characterization techniques:[1]Gel Permeation Chromatography (GPC), [2]Differential Scanning Calorimetry (DSC),[3]Nuclear Magnetic Resonance (NMR), [4]Huang-Brown model.*

| Material | Mw (kg/mol)[1] | Mw/Mn[1] (unimodal) | Crystallinity %[2] | SCB/1000C[1] | SCBD[1] | Comonomer wt%[3] | $l_c$ (nm)[2] | % Tie molecules[4] | Expected ESCR |
|---|---|---|---|---|---|---|---|---|---|
| A | 90 | Medium | 59 | 9 ÷ 11 | Uniform | 4 ÷ 6 | 14.5 | 4.4 | Medium-low |
| B | 92 | Medium | 62 | 3 ÷ 5 | Uniform | 3 ÷ 5 | 16.1 | 3.7 | Medium-high |
| C | 207 | High | 64 | 7 ÷ 9 | SCBs at high M | 2 ÷ 5 | 16.1 | 5.7 | Excellent |
| D | 78 | Medium | 85 | - | - | - | 29.4 | 0.9 | Low |

To minimize orientation effects in the materials, specimens were prepared from pellets using compression molding. Plates with a nominal thickness of 11 mm were produced for fracture testing, while thinner 1-3 mm plates were made for tensile tests and Bell telephone test. The compression molding process followed the procedure below:

- The pellets were heated at 170°C for 10 minutes.

- A pressure of about 2.5 MPa was applied for 5 minutes while keeping the temperature constant at 170°C.

- The pressure was increased to about 5 MPa for another 5 minutes, keeping the temperature constant at 170°C.

- While maintaining the 5 MPa pressure, the temperature was gradually reduced to room temperature. To prevent the buildup of thermal stresses, a slow cooling rate of 1°C was employed in the temperature range close to crystallization.

The effect of processing was evaluated by comparing the results of DSC and XRD analyses carried out on the raw pellets and compression molded samples, as shown in Table 2. Although the low applied cooling rate resulted in a slightly higher crystallinity, materials A and B maintained similar relative levels of crystallinity degree and lamellar thickness after processing. Therefore, it is safe to assume that compression molding did not significantly alter the intended structural similarities between these two materials.

***Table 2:*** *Comparison of crystallinity (%) and lamellar thickness ($l_c$) between pellets and compression molded (CM) plates for polyethylene materials A and B, results from DSC analysis.*

| Material | Crystallinity (%) | | $l_c$ (nm) | |
|---|---|---|---|---|
| | Pellets | CM Plate | Pellets | CM Plate |
| A | 58.9 | 63.8 | 14.5 | 17 |
| B | 61.5 | 64.7 | 16.1 | 19 |

## 4. Methods

### 4.1 Uniaxial tensile tests

Type 2 [95] dumbbell specimens were die-cut from compression-molded plates having a thickness of roughly 1 mm. Tests were conducted at temperatures of 50 °C, 65 °C, and 80 °C using constant displacement rates of 2, 20, and 200 mm/min. The purpose of these tests was to determine the relaxation modulus $E(t)$ of the materials and to investigate their potentially nonlinear behavior. Tests were performed on an Instron 1185R5800 electromechanical dynamometer equipped with a thermal chamber and a 10 kN load cell. To measure specimen deformation accurately, markers were drawn along the gauge length of each specimen, and the tests were video-recorded using a 10-megapixel uEye UI 5490 SE camera. The time-dependent relaxation modulus $E(t)$ was evaluated from the engineering stress–strain (σ–$\varepsilon$) curves obtained at different displacement rates using Equation 7, derived from principles of linear viscoelasticity [96–99]:

$$\left(\frac{\partial\sigma}{\partial\varepsilon}\right)_t = E(t) \qquad (7)$$

The curves were fitted with polynomial functions to minimize data scatter during numerical differentiation. Subsequently, time–temperature superposition was applied to extend the experimental window, allowing for the construction of relevant master curves at the reference temperature of 50°C.

### 4.2 Bell telephone tests

To rank the considered materials accordingly to an industrially recognized standard, Bell Telephone Tests were conducted following ASTM D1693-21 procedure [29]. Ten notched samples of each polyethylene were subjected to bending and immersed in hard glass test tubes containing a 10% (v/v) solution of Tergitol NP9 (Nonoxynol-9) at the constant temperature of 50°C. Specimens were periodically inspected for failure (i.e. the presence of a crack visible to the naked eye). The time taken for 50% of the specimens to fail (F50) was recorded as a measure of the material's ESCR.

### 4.3 Strain Hardening Modulus tests

Following ISO 18488 [34], tensile tests were performed with the same experimental equipment listed in paragraph 4.1 at 80°C, using a constant crosshead speed of 20 mm/min. Also, in this case the strain was measured from the recorded videos, allowing an accurate measurement even beyond the material's natural draw ratio. The strain hardening modulus $< G_p >$ was determined from the slope of the true stress – stretch ($\lambda$) curve in the region beyond the natural draw ratio, specifically for $\lambda > 8$. For each grade at least 5 samples, obtained via die cutting from 2 mm thick plates, were tested to determine a standard deviation of the measurements.

### 4.4 Fracture tests

Single Edge Notched Bending (SENB) specimens, with the dimensions shown in Figure 5, were fabricated from 11 mm plates using circular saw cutting followed by milling. The specimen geometry was selected to ensure plane strain conditions, in line with previous studies on PE [18,39,41], the applicability of the LEFM approach is then verified in paragraph 6.3.

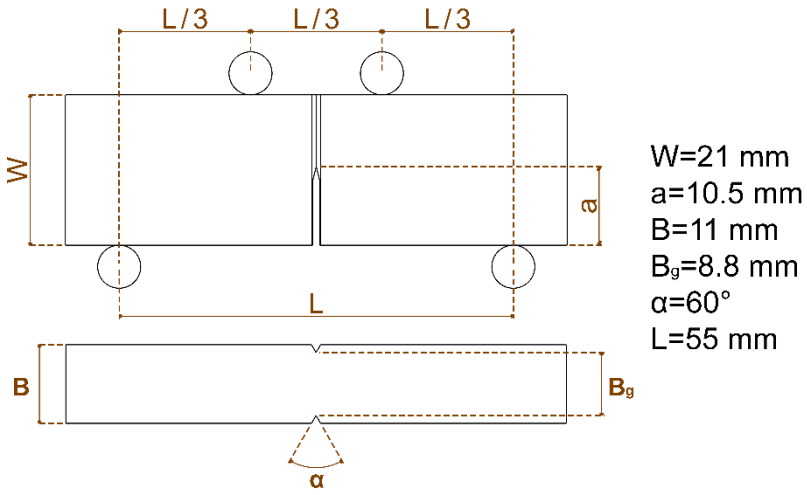


***Figure 5:*** *SENB specimen geometry and nominal dimensions used in the four-point bending configuration.*

For tests in which the specimen was subjected to a load higher than 50 N, V-shaped grooves were machined along the notch plane on both sides of the specimens to guide crack propagation and enhance constraint, aiding in the achievement of plane strain conditions [100,101]. For tests during which the specimen was subjected to a lower load it was checked that propagation occurred along the notch plane even without the presence of V-grooves. In these cases, the load required to reach a given applied stress intensity factor was higher with respect to V-grooved specimens, hence resulting in higher specimen displacement measurable with higher precision with the Linear Variable Displacement Transducer (LVDT) employed during some of the tests. The notches were introduced through automated "chisel-wise" cutting with a sharp blade, achieving a final notch root radius of less than 10 µm. In addition, a set of SENB specimens with blunt notches was prepared using a circular profile blade with a 1 mm radius. These blunt-notch specimens were used in creep tests for compliance calibration, as described in Appendix A.

SENB specimens were tested at 50°C to enable comparison with Bell Telephone test results. Two different loading histories were applied: constant displacement rates (from 0.01 to 100 mm/min) and constant loads (creep), both using the four-point bending configuration already shown in Figure 5. These loading conditions allowed for the exploration of various time ranges, with shorter tests performed on a universal testing machine and longer tests conducted on dedicated equipment. Previous studies [40,41,102,103] demonstrated that the results are independent of the applied loading history.
Fracture tests were initially carried out to determine the reference fracture behavior in air. Subsequently, the effect of an active environment was investigated by placing the specimens in flexible bags containing a 10%

(v/v) solution of Tergitol NP9, the same used for Bell Telephone tests. Constant displacement rate tests were conducted using an Instron 1185R5800 electro-mechanical dynamometer, equipped with a 10 kN load cell, with sample deflection measured directly from the crosshead displacement. The tests were monitored using a 10 Mpixel uEye UI 5490 SE camera, and crack length was measured over time to determine crack initiation and propagation speed. Backlighting was employed to improve visibility of the crack tip, even when rim films formed and hindered detection (Figure 6).

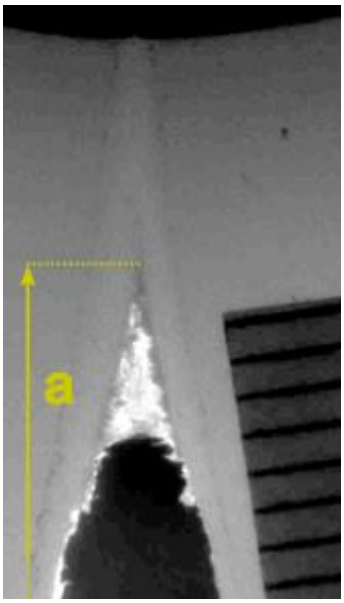


*Figure 6: A video frame captured during a fracture test, illustrating the crack propagation. The formation and evolution of a rim film obscures the direct visual identification of the crack tip. Backlighting was used to help estimate the crack tip's position through the thin film forming along the sample edge.*

Creep tests were performed on custom-built machines featuring two fixed lower pins and two upper pins, where the load was applied using a pneumatic system capable of releasing a dead weight in a controlled manner within seconds. Specimen deflection at the load pins was measured using a LVDT. A compliance calibration method was used to assess crack initiation and propagation (see Appendix A). To implement this procedure, the compliance of blunt-notched specimens tested under the same loading conditions as the fracture tests was first measured, since crack initiation does not occur within a practical timeframe in the absence of a sharp notch. With this data, along with the compliance measurements from sharp-notched specimens during fracture tests, the crack length could be determined at any point during the tests.

Characteristic initiation and propagation curves were obtained by plotting on a log-log scale both the stress intensity factor and the energy release rate versus the crack initiation time and the crack growth rate, respectively.

*Stress intensity factor*

$K$ was evaluated according to the following expression for SENB specimens in pure bending:

$$K = Y\left(\frac{a}{W}\right)\frac{PL\sqrt{\pi a}}{B^{*}W^{2}} \qquad (8)$$

Where $P$ is the applied load, $L$ is the span length and $W$ is the specimen width. The shape factor $Y\left(\frac{a}{W}\right)$ was computed according to Rooke and Cartwright [104] (see Appendix A).

An effective thickness, $B^*$, was considered in Eq. (8) to account for the presence of side grooves [100] on the stress distribution in the specimen ligament. In accordance with Andena et al. [40], $B^*$ was evaluated as:

$$B^* = B^{0.263} B_g^{0.737} \quad (9)$$

With $B$ and $B_g$ being the sample thickness of the ungrooved and grooved sections, respectively (see Figure 5). Of course, in the case of samples without grooves, Eq. (8) was considered with $B^* = B$.

*Energy release rate*

The energy release rate $G$ for constant load tests was evaluated using the approach proposed by Williams [36]:

$$G = \frac{Pu}{2B_g W} \frac{1}{\psi\left(\frac{a}{W}\right)} \quad (10)$$

Where $P$ is the applied load, $u$ is the displacement, $W$ is the specimen width, $B_g$ is the sample thickness of the grooved section and $\psi\left(\frac{a}{W}\right)$ is the calibration factor for the considered test configuration. The derivation for the latter is shown in Appendix B. In the case of samples without grooves $B_g = B$ is considered.

For constant displacement tests where uncertainties in crack onset determination can lead to large data scattering when evaluating the strain energy, G was calculated from:

$$G(t) = \frac{K(t)^2}{E(t)}(1 - \nu^2) \quad (11)$$

where $E$ is the relaxation modulus and $\nu$ is Poisson's ratio. $E(t)$ data is derived from tensile tests as explained in section 4.1.

## 5. Results

### 5.1 Evaluation of ESCR: Bell test and strain hardening modulus

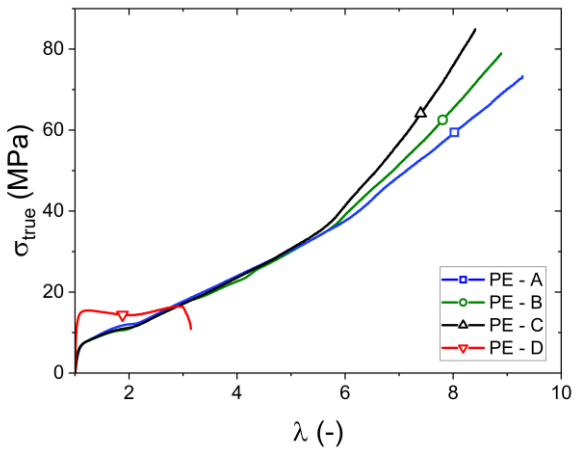


***Figure 7:*** *Examples of true stress ($\sigma_{true}$) vs stretch ($\lambda$) curves used to calculate the strain hardening modulus.*

Figure 7 shows the results of the tensile tests performed on the PE grades to measure strain hardening. In Table 3 the results of the Bell telephone test and strain hardening modulus for the four materials considered are presented. As expected, material C showed high resistance to ESC and no visible fracture on the samples

could be observed within a reasonable experimental window. Conversely, sample D did not show any strain hardening behavior after yielding and each sample broke well before reaching a stretch value of 8, as required by ISO 18488. As can be seen from Table 3 and Figure 7, these two methods provide the same ranking between the different materials.

***Table 3**: Results of the Bell test and Strain Hardening Modulus.*

| Material | Bell test F50 (h) | Strain Hardening Modulus $< G_p >$ (MPa) |
|---|---|---|
| A | 32 | 12.2 ± 1.3 |
| B | 1584 | 17.7 ± 1.1 |
| C | >5000 | 27 ± 0.8 |
| D | 2.4 | - |

### 5.2 Evaluation of ESCR: Fracture Mechanics approach

In the following, results obtained adopting a LEFM approach to quasi-static tests will be presented, first in terms of crack initiation, and subsequently of crack propagation.

#### *5.2.1 Crack initiation*

Figure 8 shows plots of the stress intensity factor ($K$) and energy release rate ($G$) against crack initiation time ($t_i$) for each material tested in air and in presence of a 10% (v/v) solution of Tergitol NP9. Data from individual tests are represented by solid (air) and hollow points (active environment) in a log-log scale, with interpolating lines drawn using a best-fit algorithm (typically with an $R^2$ value greater than 0.8). Figure 9 provides a comparative analysis across all materials, prioritizing clarity by omitting individual data points.

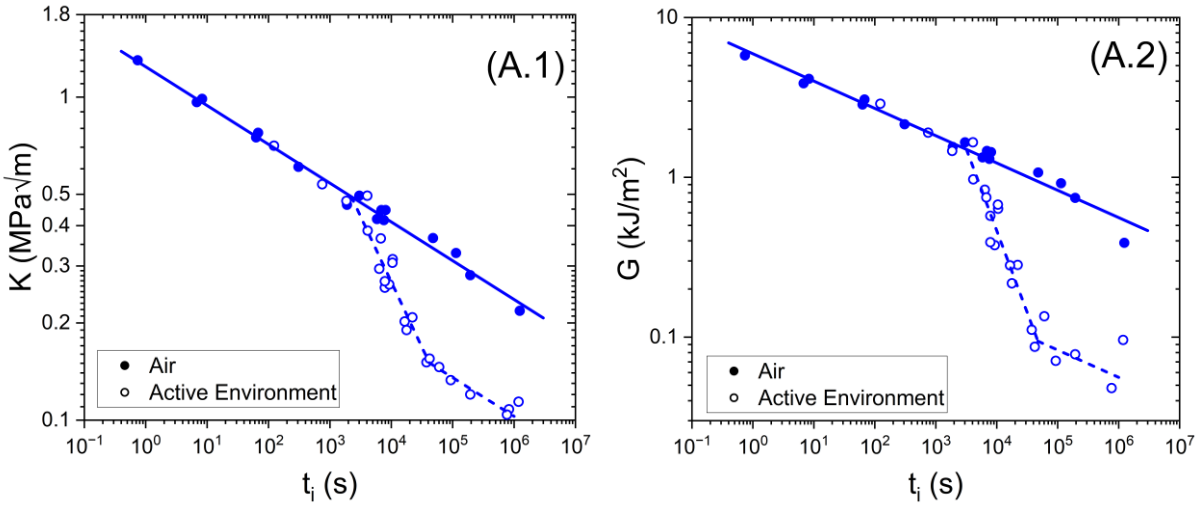

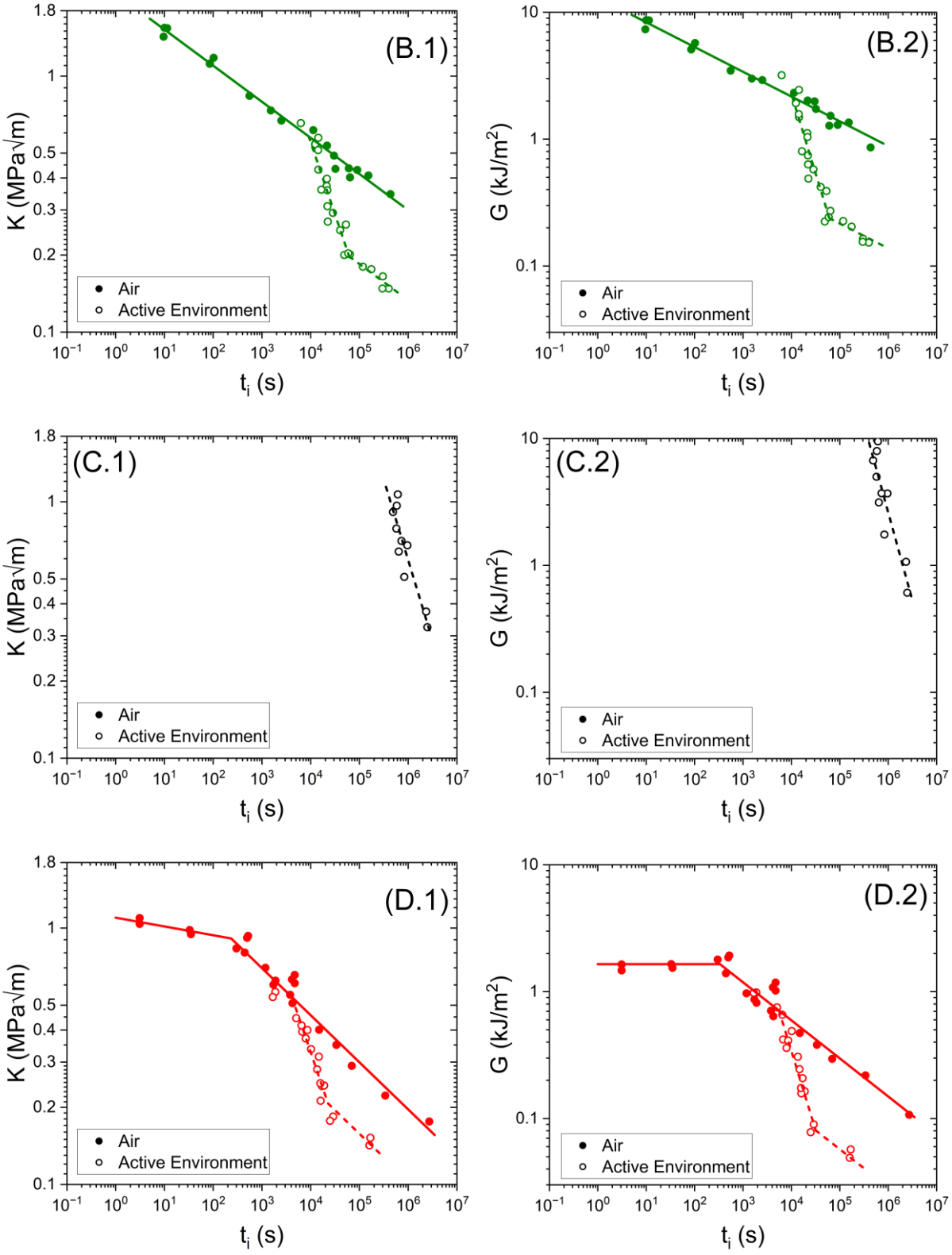


***Figure 8***: *Crack onset graphs for materials A, B, C, and D, showing K (A.1, B.1, C.1, D.1) and G (A.2, B.2, C.2, D.2) versus $t_i$ in air (solid points) and active environment (hollow points). All tests were conducted at* $50°C$.

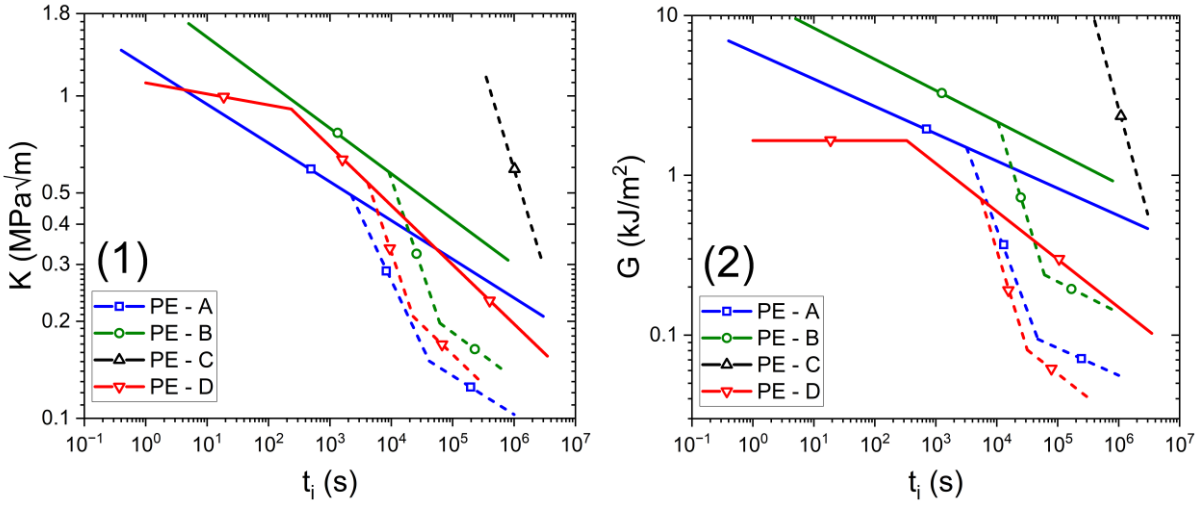


***Figure 9:*** *Comparison of K (1) and G (2) vs. $t_i$ for polyethylene materials A, B, C, and D. All tests were conducted at* $50°C$*. The solid lines represent behavior in air, while the dashed lines correspond to tests conducted in active environment.*

### *5.2.2 Crack Propagation*

Figure 10 presents plots of the stress intensity factor $(K)$ and energy release rate $(G)$ versus crack speed $\left(\frac{da}{dt}\right)$ for each material. Solid points represent the test data, fitted using a power law equation on a log-log scale. Figure 11 offers a comprehensive comparison of trends across the materials, once again omitting the experimental data. Data for material C has been excluded from detailed analysis due to its exceptionally high resistance to crack propagation, which resulted in discontinuous crack growth behavior under the test conditions (Figure 12). This type of behavior has been observed by other authors studying tough grades of PE [105–107].

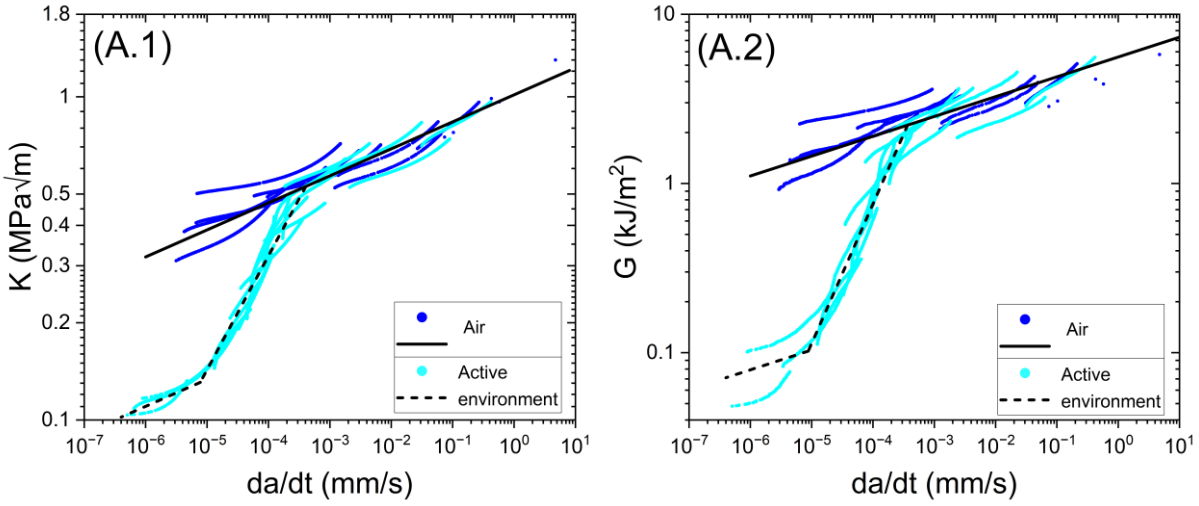

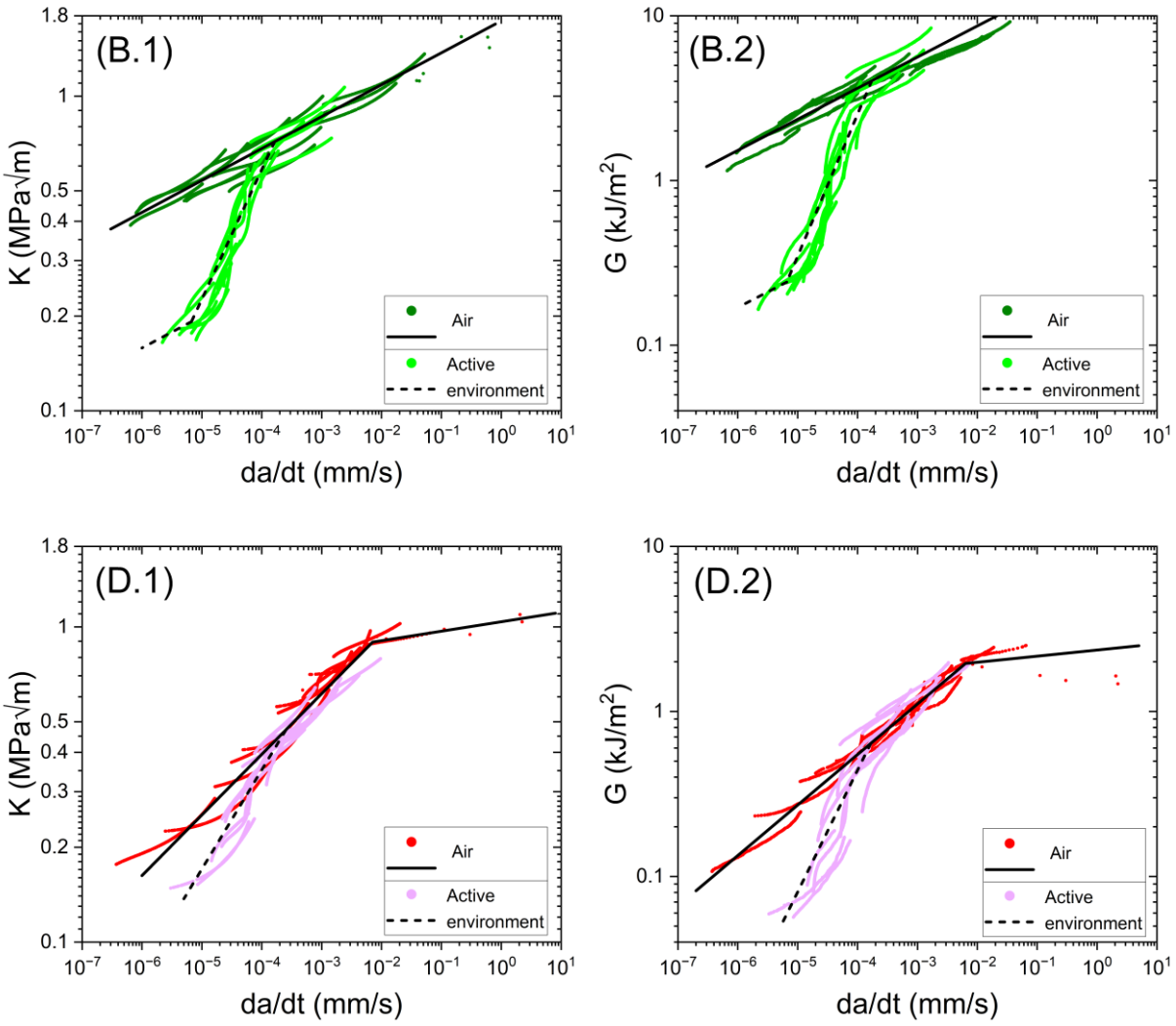


***Figure 10:*** *Crack propagation graphs for materials A, B, and D, showing K (A.1, B.1, D.1) and G (A.2, B.2, D.2) versus crack growth rate (da/dt) in air and active environments. All tests were conducted at* 50°C.

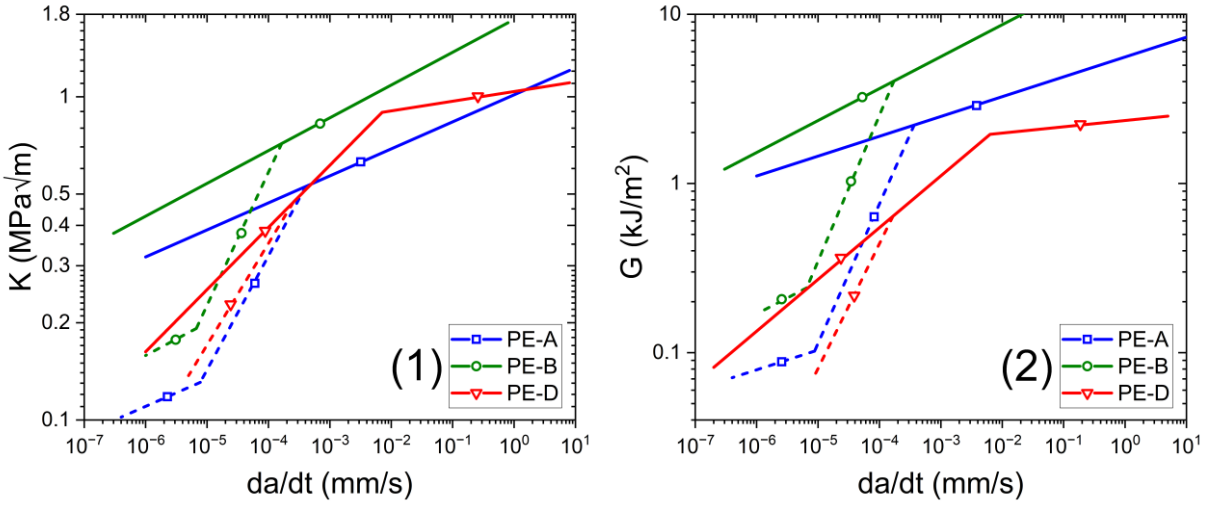


***Figure 11:*** *Comparison of K (1) and G (2) vs. crack growth rate (da/dt) for polyethylene materials A, B, and D. All tests were conducted at* 50°C. *The solid lines represent behavior in air, while the dashed lines correspond to tests conducted in an active environment.*

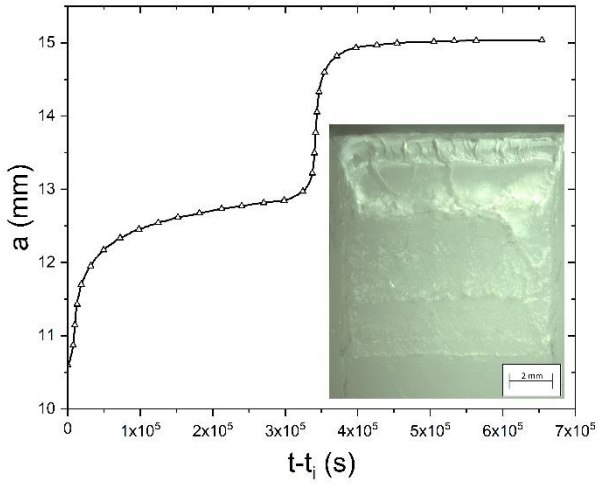


***Figure 12:*** *Crack length (a) as a function of time after initiation (t-$t_i$) for material C, showing discontinuous crack growth. The inset shows a fracture surface with distinct zones of crack arrest.*

## 6. Discussion

### 6.1 Bell telephone test and Strain hardening modulus

The results from the Bell telephone test, strain hardening modulus, and the theoretical calculations using the H-B model provide valuable insights into the stress cracking resistance of the analyzed PE grades.

The Bell test is widely employed in the PE industry as a quality control tool due to its simplicity in sample preparation and straightforward data analysis. However, comparing results across different materials presents some challenges. In the Bell test, samples are bent and placed into test tubes, subjecting each sample to an approximately fixed strain. The stress experienced by each material is directly related to its stiffness, with the relaxation modulus being the key property for viscoelastic materials.

For the materials considered, reference values of the relaxation moduli obtained from uniaxial tensile tests are provided in table 4:

***Table 4:*** *Relaxation modulus (E) values for polyethylene materials A, B, C, and D at 50°C, ε = 0.1%, and t = 0.1 s.*

| Material | $E\ (MPa)$ |
|---|---|
| A | 268 ± 8 |
| B | 318 ± 24 |
| C | 317 ± 12 |
| D | 839 ± 22 |

Materials A, B, and C (LLDPEs with similar crystallinity) exhibit comparable stiffness, while material D (HDPE) is significantly stiffer. Under the typical conditions of a Bell test, it is reasonable to assume that materials A, B, and C experience similar stress fields, making their test results directly comparable. However, material D is subjected to a stress field 2-3 times greater than the other materials, potentially introducing a bias in the test results for this material.

A key observation from the Bell test results is that material B demonstrated significantly higher ESCR compared to material A, even though both materials share nearly identical microstructural parameters, such as molecular weight and lamellar thickness. Interestingly, the H-B model (Table 1) predicted a higher concentration of tie molecules for material A. The critical difference between the two lies in the type and content of the comonomer. Material B, with lower comonomer content, exhibits superior resistance to ESC.

This suggests that, despite the similar bulk properties of materials A and B, the superior performance of LLDPE 1-hexene in resisting SCG and ESC can be primarily attributed to the longer chain length of the 1-hexene comonomer, rather than other microstructural factors. This important finding highlights the critical role of comonomer chain length in enhancing ESCR, even when other structural parameters are comparable. The strain hardening modulus also reflects this behavior with material B displaying a higher value of $< G_p >$ than material A. This indicates that, despite their similar morpho-structural features, the two materials exhibit a notable difference in the density of stress transmitters between lamellae. It remains unclear whether this difference can be attributed solely to tie molecules or if other factors, such as entanglement density, also play a role.

Additionally, the results emphasize the importance of molecular weight as a dominant factor in determining ESCR. This is particularly evident when comparing material C with the other grades. Material C exhibited significantly higher ESCR, with its F50 value exceeding the limits of the experimental window, indicating an exceptionally high resistance to SCG. The key distinction lies in its substantially higher molecular weight compared to materials A and B. Higher molecular weight allows for the formation of more tie molecules, this effect is highlighted by the higher percentage of tie molecules predicted by the H-B model for material C. Moreover, the strain hardening modulus provides additional insight into the material's superior performance. Material C displays the highest $< G_p >$ value among the considered grades, indicating a denser network of entanglements and tie molecules within the amorphous region.

The evaluation of the performance of material D requires careful interpretation. On one hand, its low value of F50 can likely be attributed to the material's high rigidity. On the other hand, the predicted low percentage of tie molecules and the strain hardening test results suggest that material D has inherently poor resistance to SCG and ESC. The lack of strain hardening behavior further supports this conclusion. As described by Seguela [108], a polymer's ability to stabilize necking and exhibit strain hardening depends on the balance between strain-softening, caused by lamellar fragmentation, and strain-hardening, due to the formation of a fibrillar structure. If a polymer does not possess adequate molecular weight, crystallinity, or tie-molecule density, it may fail before reaching the natural draw ratio, as it lacks the necessary support for strain hardening.

Taking all these factors into account, it is clear that material C demonstrates the highest performance, primarily due to the combination of its high molecular weight and short chain branches that enable the creation of an efficient network of tie molecules between lamellae. Materials A and B exhibit a surprising pattern, with material B significantly outperforming material A. This difference can be attributed primarily to the different comonomers used in their copolymerization. Lastly, despite the challenges in directly comparing Bell test results, material D shows the poorest resistance to SCG and ESC. Although its molecular weight is comparable to that of materials A and B, its high crystallinity and lamellar thickness hinder the formation of tie molecules relative to its molecular weight, contributing to its inferior performance.

### 6.2 LEFM tests

As highlighted in the previous section, industrial tests for ranking ESCR struggle to provide a reliable criterion for material comparison; moreover, the transferability of the results to the design of real-life components is often questionable, since the actual loading conditions may differ considerably. This is why the insights offered by the application of a FM-based approach are important: by offering a comprehensive picture of the material toughness through the parameters $K$ and $G$ it is possible to evaluate intrinsic material properties and their dependence on time and different environments. The results can then be used to predict the lifetime of products and components exposed to aggressive environments.

When examining the data from the tests, it is important to remark why both $K$ and $G$ were included in the analysis: in principle, the two fracture parameters are equivalent within the context of LEFM, and related (in plane strain conditions) by Equation 11. By comparing a criterion based on strain energy and another based

on the applied stress, a more thorough understanding of how a material may perform in different scenarios can be gained. Additionally, using both parameters together adds an extra layer of robustness to the analysis, since they can be independently determined from the experimental results.

#### *6.2.1 Behavior in air*

Considering the tests conducted in air (Figure 9), the first critical point to address is the high toughness of material C – this could be expected based on the previously shown results. Due to its superior toughness, it could only be tested in an active environment. Testing this material under LEFM assumptions in air would have necessitated samples of impractically large sizes or testing over unfeasibly long timeframes; both solutions fall outside the scope of the present study. While Elastic Plastic Fracture Mechanics (EPFM) might offer an alternative method for such cases, its framework again lies outside the focus of this article, so only active environment data are presented for grade C. This alone is a strong indication of the exceptional toughness possessed by material C and reinforces our preliminary findings.

Comparing crack initiation of materials A and B, their performance differs substantially. Under identical $K$ or $G$ values, the onset of crack growth varies roughly by an order of magnitude, a result consistent with data from the Bell Telephone test. At 50°C and over the timescales considered, grades A and B display a purely brittle fracture behavior.

Material D, on the other hand, exhibits a distinct "knee point" in its toughness curves for both $K$ vs $t_i$ and $G$ vs $t_i$ graphs, signaling a transition from ductile to brittle behavior. Its toughness exceeds what was initially suggested by the Bell telephone test, confirming the limitations of this industry-standard ranking system. When examining the relevant $K$vs $t_i$ graph (Figure 9 – (1)), it becomes evident that material D can outperform grade A under certain loading conditions. However, the energy release rate graph provides a more comprehensive view of the material's behavior, as it inherently accounts for its stiffness through the definition of $G$ itself. This graph (Figure 9 – (2)) clearly shows that material D undergoes significantly less deformation before fracture initiates. By analyzing the $K$ vs $t_i$ graph, a clearer ranking of SCG resistance emerges: Grade C >> Grade B >> Grade A ~ Grade D. When comparing Grades A and D, it is important to note that Grade A performs slightly better at lower stress intensity factors, likely due to its higher concentration of tie molecules. In contrast, at intermediate K values, material D appears to be the superior option, possibly due to its higher crystallinity. However, regardless of the applied K, Material D consistently absorbs less energy before fracturing compared to the other grades. This is reflected in the $G$ vs $t_i$ graph, leading to a well-defined fracture energy ranking of: Grade C >> Grade B >> Grade A >> Grade D.

When considering crack propagation, the behavior was analyzed by fitting the experimental crack growth vs. time curves to an analytic function. This fitting provided sufficient accuracy for evaluating the crack speed (da/dt) while filtering the experimental noise. The creep tests performed during crack propagation ensured a constant applied load, while the defect size and therefore the stress intensity factor and the energy release rate increased over time. Consequently, these tests generated a large number of data points, allowing for the observation of transitions between different propagation behaviors.

From Figure 11 it is clear that material A exhibited significantly higher crack propagation rates compared to Material B. In air, the crack speed of Material A was approximately two orders of magnitude higher than that of Material B under comparable loading conditions. This pronounced difference can be again attributed to the respective comonomer types. This mirrors the trends observed during crack initiation, where Material B consistently outperformed Material A in terms of resistance to crack onset. The HDPE homopolymer (Material D) displayed the poorest performance in terms of crack propagation speed, as observed with respect to crack initiation. The high crystallinity of HDPE leads to a relatively low number of tie molecules and their absence significantly accelerates crack growth.

*6.2.2 Behavior in active environment*

The presence of an active environment significantly influences the behavior of the materials. Both the stress intensity factor and the energy release rate required to initiate crack growth are notably lower when an active environment is present. Alternatively, for a given applied stress level, the initiation time decreases drastically. This effect becomes particularly evident for initiation times longer than $10^3$ to $10^4$ seconds. Below this threshold, little to no noticeable difference is observed between the behavior of materials in air and those exposed to an active environment. This minimum characteristic time is required for the environmental agent to diffuse into the polymer craze and begin interacting with its structure.

Once the environment has had sufficient time to interact with the polymer, a significantly lower stress intensity factor is required for crack initiation to occur in a given time. This phenomenon can be explained following the scheme outlined by Williams [36,109] in his description of environmental stress cracking (Figure 13). In the absence of an active environment, crack initiation typically follows a power-law relationship between the stress intensity factor and the time to crack initiation. However, when an active environment is present, the material's resistance to crack initiation decreases, as evidenced by the lower $K$ values needed to initiate cracks in the same time frame. This shift in behavior is attributed to a flow-controlled mechanism, where the environment interacts with the polymer at the crack tip, reducing the cohesive strength. In this scenario, the environmental agent gradually penetrates the polymer's craze fibrillar structure through diffusion, weakening the material at the craze tip. The fibrils within the craze become plasticized, reducing their resistance to fracture. This weakening mechanism is driven by the flow of the environmental agent into the porous zone at the crack tip and can be described by Darcy's Law for porous media:

$$Q = -\frac{k}{\eta}\nabla p \qquad (12)$$

Where $Q$ is the flow rate, $\nabla p$ is the pressure gradient, $k$ is the permeability of the medium, which depends on the pore area in the crazes and $\eta$ is viscosity of the fluid. The flow of the environmental agent is governed by this pressure gradient. As the agent infiltrates the craze zone, the cohesive forces within the polymer are reduced, facilitating crack initiation. This diffusion mechanism primarily affects the craze region, which has a very high area-to-volume ratio, leading to a complete plasticization of the small ligaments within a relatively short time. The steeper slopes in the graphs for tests conducted in the presence of an environment reflect this accelerated crack initiation. The environmental agents lower the critical stress intensity required for crack initiation by weakening the molecular structure at the crack tip. Consequently, crack onset occurs earlier and at lower stress levels compared to the "without environment" condition. The "knee point" in the graphs, where the slope of the curve returns to a gentler gradient, marks a transition where the environmental agent has fully exerted its accelerating effect. This phenomenon likely occurs when the environmental agent has time to completely saturate the craze structure; at this point, a constant acceleration factor (compared to the situation when the agent is not present) leads to a recovery of the original slope of the initiation curve.

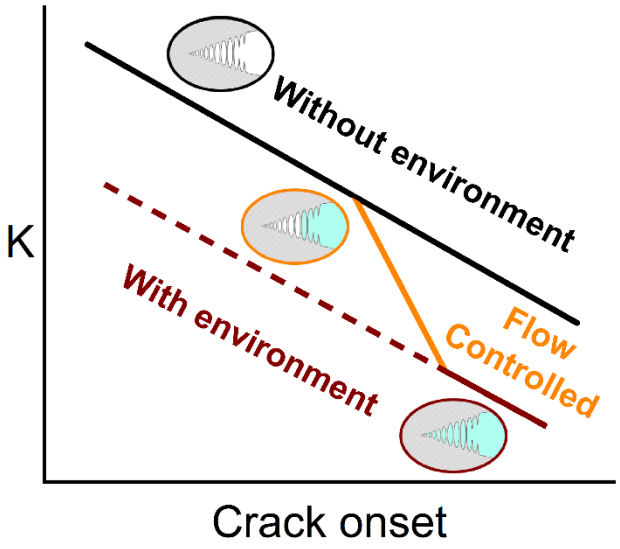


***Figure 13:*** *Schematic of crack onset behavior with and without an active environment. The black line represents crack onset in air, while the dashed line shows the reduction in fracture toughness due to full plasticization of the craze structure in an active environment. The orange line illustrates the transition to flow-controlled behavior as environmental agents begin penetrating the craze, accelerating fracture initiation.*

The same behavior was observed during the propagation phase. In the presence of an active environment, all materials experienced a reduction in crack resistance, with faster crack growth observed below a threshold of applied $K$ and $G$. The relative performance of each material remained consistent with the one observed in air. Material B continued to exhibit superior resistance to crack propagation, while Material A showed significantly higher crack speeds. The HDPE homopolymer's crack propagation rate also increased in the active environment, further highlighting its vulnerability to stress cracking.

As discussed in the section on crack initiation, the presence of an active environment accelerates the process through a diffusion-controlled mechanism. Crack propagation follows a similar pattern. While crack initiation is driven by the early interaction between the environment and the polymer, crack propagation extends this process, as the environmental agents continue to infiltrate the porous craze zone at the crack tip. In both phases, diffusion plays a critical role. During crack propagation, the environmental agent further reduces the cohesive strength of the craze fibrils as it plasticizes the fibrils. The rate of crack growth is governed by the flow of environmental agents into the craze structure, determined by the structural properties of the craze and the viscosity of the medium, as previously discussed. Crack propagation data indicate a point where the effect of the environment fully exerts its accelerating effect, visualized again by the "knee point" in the propagation curves. Once complete plasticization of the craze fibrils is reached, the acceleration of the crack growth rate becomes constant, and the original time/rate dependence originated by the material's inherent viscoelasticity is recovered.

While such a behavior had been originally predicted long ago [109], there are not many works in recent literature in which experimental data supporting this interpretation are provided. The reason is not simply related to the relatively small numbers of researchers dealing with ESC of polymers, but also to the experimental challenges related to obtain good and accurate data over a sufficiently broad time window (typically at least 4-5 decades).

### 6.3 Applicability of LEFM to PE

To verify the applicability of the adopted LEFM approach, the actual degree of nonlinearity in the materials was evaluated through tensile testing. As detailed in Section 4.1, the relaxation modulus $E(t)$ was calculated for each material using the time–temperature superposition principle. Although PE is not strictly a

thermorheologically simple material, from an engineering perspective this method provides a reasonable estimate of the relaxation modulus.

From the measured values of $E(t)$ at various strains, a threshold strain was identified. Below this threshold, the relaxation modulus remained independent of the applied strain, indicating a linear viscoelastic behavior. Above, nonlinear effects became significant. The experimental data were then fitted within the linear region using a power-law model to describe the material behavior. An example of this procedure is shown in Figure 14.

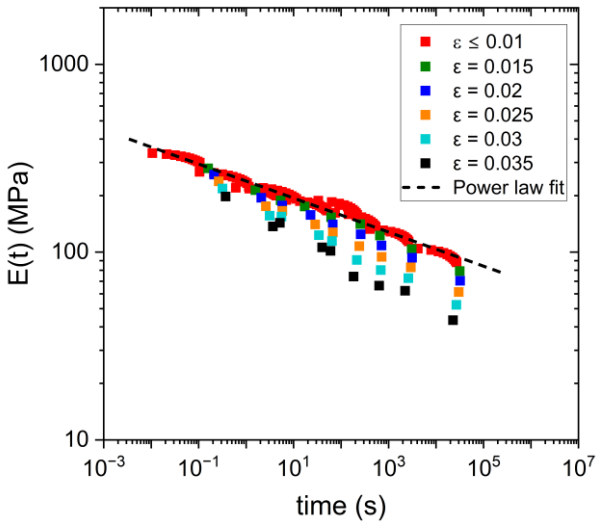


***Figure 14:*** *Example of master curve construction at 50°C for Material A using the tangent modulus from tests at 50°C, 65°C, and 80°C. The plot illustrates the transition from linear to nonlinear viscoelastic behavior across different strain levels. Points marked in red (ε < 1%) are within the linear region. A power-law fit has been applied to the linear viscoelastic region to capture the material's response.*

To verify the applicability of the LEFM approach for the materials under study, the relaxation modulus E(t) was also evaluated using data from fracture tests. This involved a comparison of the stress intensity factor $K$ and energy release rate $G$ calculated independently for the creep data. These calculations were then compared to the moduli determined from tensile tests, as discussed in Section 4.1.

Even though the time-dependent behavior of Poisson's ratio $\nu$ could contribute to the viscoelastic response, the potential variations of $\nu$ over time were deemed to have minimal impact, compared to the more significant changes in $K$ and $G$ during fracture. Therefore, for the sake of simplicity, a constant value of $\nu = 0.4$ was assumed throughout the analysis. For each tested specimen, the values of $K$ and $G$ at the point of crack initiation were used to compute the corresponding effective relaxation modulus $E(t_i)$, where $t_i$ is the crack initiation time. These effective moduli were then compared in Figure 15 against the experimental time-dependent modulus curves obtained from the tensile tests using Eq. (7).

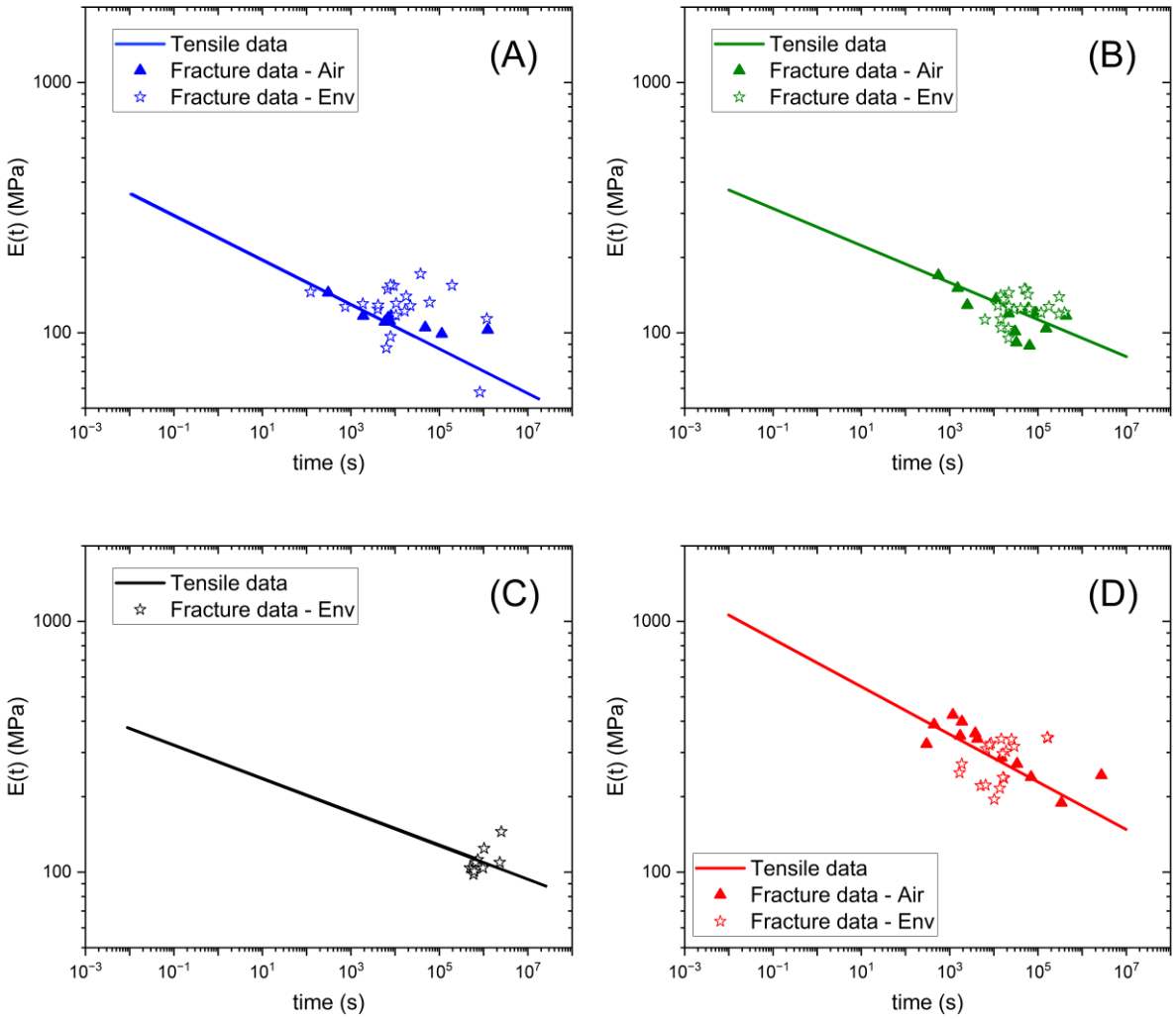


***Figure 15:*** *Comparison of relaxation modulus obtained from tensile tests and effective modulus calculated from fracture tests for materials A, B, C, and D.*

Within the reported data scatter, the moduli derived from the fracture data are quite consistent with those obtained from the tensile tests. The viscoelastic material behavior across different testing configurations is unaltered, even for material C: despite its high toughness, at low stresses its failure can still be described by a LEFM approach. One key observation is that the presence of the active environment does not appear to influence the viscoelastic properties of the material (i.e. the two sets of data in air and environment overlap). This is in accordance with the existing knowledge reported in the literature: the environmental agent primarily interacts with the localized region around the crack tip, particularly within the craze zone, thanks to the huge surface area in this region. The active environment facilitates plasticization and weakening of the craze fibrils at the crack tip, accelerating crack initiation and growth. However, this process has limited impact on bulk material properties like $E(t)$. These results support the validity of applying LEFM to nonlinear viscoelastic materials such as polyethylene under low-stress fracture conditions: despite the inherent nonlinearities in polyethylene's viscoelastic behavior, the failure strain likely remains within the threshold of linearity, particularly for cases of low-stress crack growth. The fact that both $K$ and $G$ data from the fracture tests fall on the same master curve as the tensile test results further underscores that LEFM provides an accurate framework for describing the behavior of the material in these conditions.

## 7. Conclusions

This section summarizes the main findings of this research paper.

Advantages of LEFM Over Traditional Testing Methods

The application of LEFM has proven essential in drawing meaningful comparisons between materials, offering clearer and richer information compared to traditional tests like the Bell Telephone. While the Bell test is widely used in industry, its results are sensitive to the intrinsic viscoelastic properties of each material, such as relaxation modulus, leading to biases when comparing materials with differing stiffness. LEFM, by contrast, allows for a comprehensive evaluation of the intrinsic fracture properties, enabling quantitative comparisons even between grades with markedly different properties. Moreover, the data provided by LEFM can be directly used for design and evaluation of engineering structures.

Impact of Morpho-Structural Parameters on SCG

The results confirm that molecular weight is a primary determinant of polyethylene's resistance to SCG and ESC. Higher molecular weight facilitates the formation of tie molecules, significantly enhancing crack resistance. This effect has been accurately quantified: material C, with its high molecular weight, outperformed all other grades, exhibiting remarkable resistance to SCG, also in presence of the aggressive environment. The study also highlights the significant impact of comonomer type on stress cracking resistance. Materials A and B, despite similar molecular weights and crystallinities, displayed markedly different crack resistance due to their comonomer types. This suggests that the length of the side chain in the comonomer plays a crucial role in enhancing SCG resistance. The introduction of side chains having different lengths may potentially lead to variations in tie molecule formation or in the density of chain entanglements within the amorphous regions. However, these mechanisms are not fully understood, and conflicting results have been reported in the literature. Therefore, further research is necessary to explain the underlying mechanisms, possibly through advanced characterization techniques and molecular dynamics simulations.

Environmental Stress Cracking Behavior

The behavior of PE with respect to environmental stress cracking revealed three distinct regimes of fracture behavior, depending on the applied stress intensity factor, material properties, and environmental agent:

- No environmental interaction: the material's inherent viscoelastic properties govern crack initiation and propagation (no plasticization of the craze fibrils).
- Partial plasticization: environmental agents begin to interact with the polymer at the crack tip, reducing cohesive strength and affecting the fracture process.
- Full plasticization: environmental agents permeate the craze zone, leading to complete plasticization of the craze fibrils and markedly accelerated crack initiation and propagation.

These findings support a previous model proposed by Williams [36,109]; however, conflicting results have been reported regarding the impact of environmental agent concentration and viscosity on ESC [38,44,45]. Further experimental work will be necessary to verify the model and improve the predictability of ESC behavior.

Final Remarks

In conclusion, this study advances the understanding of how morpho-structural parameters and environmental conditions collectively influence the fracture behavior of polyethylene. The proposed LEFM-based approach is not a mere phenomenological tool to evaluate ESCR but can be leveraged to provide valuable insights that can inform the design and optimization of polyethylene materials for enhanced long-term performance in industrial applications.

## 8. Appendices

### Appendix A - compliance calibration method

Without a direct visual observation of the crack, compliance analysis allows the instantaneous crack length determination. Compliance, defined as the ratio of recorded displacement to applied load, is monitored over time for a notched specimen. Initially, the increase in compliance is governed by viscoelastic creep. However, once the crack initiates, the change in compliance is also influenced by crack propagation. To accurately determine crack length, the viscoelastic contribution must be subtracted first.

For a linear elastic material under plane strain, the following relationship describes the compliance change with respect to defect size [110]:

$$\frac{d\mathrm{C}}{da} = \frac{2B}{P^2}\frac{K^2}{E}(1-\nu^2) \quad (13)$$

where C is the sample compliance, $a$ is the defect size, $B$ is the sample thickness, $P$ is the applied load, $E$ Is Young's modulus and $\nu$ is Poisson's ratio. For polymeric materials, which exhibit time-dependent creep, this expression can be modified as follows:

$$\frac{d\mathrm{C}}{da} = \frac{2BK^2}{P^2}D(t)(1-\nu^2) \quad (14)$$

Here $D(t)$ represents the time-dependent creep compliance of the material. Integrating this expression yields:

$$C(a,t) = C(0) + \int_0^a \frac{2BK^2}{P^2}D(t)(1-\nu^2)da \quad (15)$$

In this integral $C(0)$ denotes the initial compliance of a specimen without any defect:

$$C(0) = \frac{\Delta_{FPB}}{P} \quad (16)$$

where $\Delta_{FPB}$ is the deflection of a beam in a four-point bending (FPB) setup. For a Timoshenko beam, which correctly accounts for shear effects, $\Delta_{FPB}$ can be computed as [111,112]:

$$\Delta_{FPB} = \frac{2}{5}\frac{PL}{EBW}(1+\nu) + \frac{5}{27}\frac{PL^3}{EBW^3} \quad (17)$$

In the case of FPB, $K$ can be evaluated using Eq. 8 and the shape factor $Y\left(\frac{a}{W}\right)$ for pure bending can be computed as [104]:

$$Y\left(\frac{a}{W}\right) = 1.12 - 1.39\left(\frac{a}{W}\right) + 7.32\left(\frac{a}{W}\right)^2 - 13.1\left(\frac{a}{W}\right)^3 + 14.0\left(\frac{a}{W}\right)^4 \quad (18)$$

The combination of Eq. 8 and 18 into eq. 15 leads to an analytical expression for $C$:

$$C\left(\frac{a}{W},t\right)=D(t)\frac{L}{BW}\left\{\frac{2(1+\nu)}{5}+\frac{5L^2}{27W^2}+2(1-\nu^2)\frac{\pi L}{W}\left(0.6272\left(\frac{a}{W}\right)^2-1.0379\left(\frac{a}{W}\right)^3+4.5822\left(\frac{a}{W}\right)^4-9.9387\left(\frac{a}{W}\right)^5+20.2267\left(\frac{a}{W}\right)^6-32.9577\left(\frac{a}{W}\right)^7+47.0713\left(\frac{a}{W}\right)^8-40.7556\left(\frac{a}{W}\right)^9+19.6\left(\frac{a}{W}\right)^{10}\right)\right\} \quad (19)$$

The previous equation can then be rewritten for clarity as:

$$C\left(\frac{a}{W},t\right)=D(t)\phi\left(\frac{a}{W}\right) \quad (20)$$

The material's compliance $D(t)$ can be obtained with any kind of independent measurement. For the case of SENB specimens, blunt notched specimens were used to evaluate the viscoelastic contribution (creep) to the compliance of identically sized sharp notched ones. In this way, the stress state of the actual fracture samples is accurately reproduced.

From each fracture sample an apparent compliance $D^*(t)$ is computed:

$$D^*(t)=\frac{\phi\left(\frac{a_0}{W}\right)}{C\left(\frac{a}{W},t\right)} \quad (21)$$

where $a_0$ is the initial crack length. This property will be equal to $D(t)$ until fracture onset, and then it will diverge due to the growing crack. To determine crack initiation the following criterion was adopted:

$$\frac{D^*(t)}{D(t)}\geq 1.01 \quad (22)$$

To obtain the data on crack length vs. time, the following equation was solved for each experimental point after initiation:

$$D^*(t)\,\phi\left(\frac{a(t)}{W}\right)=D(t) \quad (23)$$

**Appendix B - Energy release rate calibration function**

$\psi\left(\frac{a}{W}\right)$ is called energy calibration function and can be calculated as [36]:

$$\psi\left(\frac{a}{W}\right)=\frac{C}{\frac{dC}{d\left(\frac{a}{W}\right)}} \quad (24)$$

The analytical expression in the case of FPB for $C\left(\frac{a}{W},t\right)$ was defined in eq. 19, therefore differentiating with respect to $\frac{a}{W}$ the value of $\psi_{FPB}\left(\frac{a}{W}\right)$ can be found as:

$$\psi_{FPB}\left(\frac{a}{W}\right) = \frac{C(a)}{\frac{dC}{d\left(\frac{a}{W}\right)}}$$
$$= \left\{\frac{2(1+\nu)}{5} + \frac{5L^2}{27W^2}\right.$$
$$+ 2(1-\nu^2)\frac{\pi L}{W}\left(0.6272\left(\frac{a}{W}\right)^2 - 1.0379\left(\frac{a}{W}\right)^3 + 4.5822\left(\frac{a}{W}\right)^4\right.$$
$$- 9.9387\left(\frac{a}{W}\right)^5 + 20.2267\left(\frac{a}{W}\right)^6 - 32.9577\left(\frac{a}{W}\right)^7 + 47.0713\left(\frac{a}{W}\right)^8 \qquad (25)$$
$$\left.\left. - 40.7556\left(\frac{a}{W}\right)^9 + 19.6\left(\frac{a}{W}\right)^{10}\right)\right\}$$
$$\cdot\left\{2(1-\nu^2)\frac{\pi L}{W}\left[1.2544\left(\frac{a}{W}\right) - 3.1136\left(\frac{a}{W}\right)^2 + 18.3289\left(\frac{a}{W}\right)^3\right.\right.$$
$$- 49.6936\left(\frac{a}{W}\right)^4 + 121.3604\left(\frac{a}{W}\right)^5 - 230.704\left(\frac{a}{W}\right)^6 + 376.57\left(\frac{a}{W}\right)^7$$
$$\left.\left. - 366.8\left(\frac{a}{W}\right)^8 + 196\left(\frac{a}{W}\right)^9\right]\right\}^{-1}$$

**Acknowledgment**

The authors would like to thank Oscar Bressan (Politecnico di Milano), Juri Menegari and Claudio Mancinelli (Versalis S.p.A.) for their technical support and assistance with testing.

**References**

[1] Wang H, Shah J, Hawwat S El, Huang Q, Khatami A. A comprehensive review of polyethylene pipes: Failure mechanisms, performance models, inspection methods, and repair solutions. Journal of Pipeline Science and Engineering 2024;4. https://doi.org/10.1016/j.jpse.2024.100174.

[2] ASTM International. Standard Test Method for Time-to-Failure of Plastic Pipe Under Constant Internal Pressure 2023. https://doi.org/10.1520/D1598-23.

[3] Krishnaswamy RK. Analysis of ductile and brittle failures from creep rupture testing of high-density polyethylene (HDPE) pipes. Polymer (Guildf) 2005;46:11664–72. https://doi.org/10.1016/j.polymer.2005.09.084.

[4] Soltaninezhad S, Salavati H, Soltani Goharrizi A. Ductile fracture assessment of high-density polyethylene (HDPE-PE100) weakened by an inclined double keyhole notch. Theoretical and Applied Fracture Mechanics 2019;104:102349. https://doi.org/10.1016/j.tafmec.2019.102349.

[5] Venizelos GP, Greenshields CJ, Ivankovic A. Creep Crack Growth in PE100 Pipe Materials. Proceedings of the 10th Plastic Pipes Conference, Göteborg, Sweden: 1998.

[6] DesLauriers PJ, McDaniel MP, Rohlfing DC, Krishnaswamy RK, Secora SJ, Benham EA, et al. A comparative study of multimodal vs. bimodal polyethylene pipe resins for PE-100 applications. Polym Eng Sci 2005;45:1203–13. https://doi.org/10.1002/pen.20390.

[7] Lustiger A, Corneliussen RD. The role of crazes in the crack growth of polyethylene. J Mater Sci 1987;22:2470–6. https://doi.org/10.1007/BF01082132.

[8] DeCoste JB, Malm FS, Wallder VT. Cracking of Stressed Polyethylene. Ind Eng Chem 1951;43:117–21. https://doi.org/doi/10.1021/ie50493a035.

[9] Brown N, Bhattacharya SK. The initiation of slow crack growth in linear polyethylene under single edge notch tension and plane strain. J Mater Sci 1985;20:4553–60. https://doi.org/10.1007/BF00559346.

[10] Altstädt V. The influence of molecular variables on fatigue resistance in stress cracking environments. Advances in Polymer Science 2005;188:105–52. https://doi.org/10.1007/b136975.

[11] Wright DC. Environmental stress cracking of plastics. Rapra Technology; 2001.

[12] Brown N, Lu X, Huang Y, Qian R. Slow crack growth in polyethylene - a review. Makromolekulare Chemie Macromolecular Symposia 1991;41:55–67. https://doi.org/10.1002/masy.19910410107.

[13] Frank A, Pinter G, Lang RW. Prediction of the remaining lifetime of polyethylene pipes after up to 30 years in use. Polym Test 2009;28:737–45. https://doi.org/10.1016/j.polymertesting.2009.06.004.

[14] Zhang Y, Jar P-Y Ben. Comparison of Mechanical Properties Between PE80 and PE100 Pipe Materials. J Mater Eng Perform 2016;25:4326–32. https://doi.org/10.1007/s11665-016-2274-2.

[15] Almomani A, Mourad AHI, Deveci S. Effect of the crack layer theory parameters on the discontinuous slow crack growth of high density polyethylene under fatigue loading. Int J Solids Struct 2024;286–287. https://doi.org/10.1016/j.ijsolstr.2023.112579.

[16] Almomani A, Mourad AHI, Deveci S, Wee JW, Choi BH. Recent advances in slow crack growth modeling of polyethylene materials. Mater Des 2023;227. https://doi.org/10.1016/j.matdes.2023.111720.

[17] Thuy M, Pedragosa-Rincón M, Niebergall U, Oehler H, Alig I, Böhning M. Environmental Stress Cracking of High-Density Polyethylene Applying Linear Elastic Fracture Mechanics. Polymers (Basel) 2022;14. https://doi.org/10.3390/polym14122415.

[18] Contino M, Andena L, Rink M. Environmental stress cracking of high-density polyethylene under plane stress conditions. Eng Fract Mech 2021;241. https://doi.org/10.1016/j.engfracmech.2020.107422.

[19] Kovar M, Nezbedova E, Hodan J, Stary Z. Strain Hardening Test: Short Term Test for Estimating Service Life of High-Density Polyethylene. Macromol Symp 2022;403. https://doi.org/10.1002/masy.202200056.

[20] International Organization for Standardization. Plastics — Determination of environmental stress cracking (ESC) of polyethylene — Full-notch creep test (FNCT) 2019.

[21] International Organization for Standardization. Plastics — Notch tensile test to measure the resistance to slow crack growth of polyethylene materials for pipe and fitting products (PENT) 2005.

[22] Frank A, Bruckmoser K, Redhead A, Gruber DP, Pinter G. Investigation of the Slow Crack Growth Behavior of Static and Cyclic Loaded Specimens of Polyethylene by 2D and 3D Optical Fracture Surface Analysis. Macromol Symp 2012;311:103–11. https://doi.org/10.1002/masy.201000097.

[23] Frank A, Arbeiter FJ, Berger IJ, Hutař P, Náhlík L, Pinter G. Fracture Mechanics Lifetime Prediction of Polyethylene Pipes. J Pipeline Syst Eng Pract 2019;10. https://doi.org/10.1061/(ASCE)PS.1949-1204.0000356.

[24] Trávníček L, Poduška J, Messiha M, Arbeiter F, Pinter G, Náhlík L, et al. Effect of recycled material on failure by slow crack growth in multi-layer polyethylene pipes. Eng Fract Mech 2023;289:109423. https://doi.org/10.1016/j.engfracmech.2023.109423.

[25] Redhead A, Frank A, Pinter G. Investigation of slow crack growth initiation in polyethylene pipe grades with accelerated cyclic tests. Eng Fract Mech 2013;101:2–9. https://doi.org/10.1016/j.engfracmech.2012.09.022.

[26] Frank A, Pinter G. Cyclic Cracked Round Bar Test: Final Results of International Round Robin Test 2014. https://doi.org/10.13140/RG.2.1.1817.6400.

[27] Frank A, Berger I, Arbeiter F, Pinter G. The Cyclic Cracked Round Bar Test as a new standard for accelerated material ranking of polyethylene pipe grades, 2017.

[28] International Organization for Standardization. Polyethylene (PE) materials for piping systems – Determination of resistance to slow crack growth under cyclic loading – Cracked Round Bar test method 2015.

[29] ASTM International. Standard Test Method for Environmental Stress-Cracking of Ethylene Plastics 2021. https://doi.org/10.1520/D1693-21.

[30] Havermans-van Beek DJML, Deblieck R. Strain Hardening: An Elegant and Fast Method to Predict the Slow Crack Growth Behavior of HDPE Pipe Materials. Society of Plastics Engineers EUROTEC Conference 2011.

[31] Domínguez C, Robledo N, Paredes B, García-Muñoz RA. Strain hardening test on the limits of Slow Crack Growth evaluation in high resistance polyethylene resins: Effect of comonomer type. Polym Test 2020;81. https://doi.org/10.1016/j.polymertesting.2019.106155.

[32] Kurelec L, Teeuwen M, Schoffeleers H, Deblieck R. Strain hardening modulus as a measure of environmental stress crack resistance of high density polyethylene. Polymer (Guildf) 2005;46:6369–79. https://doi.org/10.1016/j.polymer.2005.05.061.

[33] Cheng JJ, Polak MA, Penlidis A. A tensile strain hardening test indicator of environmental stress cracking resistance. Journal of Macromolecular Science, Part A: Pure and Applied Chemistry 2008;45:599–611. https://doi.org/10.1080/10601320802168728.

[34] International Organization for Standardization. Polyethylene (PE) materials for piping systems — Determination of Strain Hardening Modulus in relation to slow crack growth — Test method 2015.

[35] Kinloch AJ, Young RJ. Fracture behaviour of polymers. London; New York, NY, USA: Applied Science Publishers; Sole distributor in the USA and Canada, Elsevier Science Pub. Co.; 1983.

[36] Williams JG. Fracture Mechanics of Polymers. Chichester, New York: Ellis Horwood; 1984.

[37] Schapery RA. A theory of crack initiation and growth in viscoelastic media. Int J Fract 1975;11:141–59. https://doi.org/10.1007/BF00034721.

[38] Rink M, Frassine R, Mariani P, Carianni G. Effects of Detergent on Crack Initiation and Propagation in Polyethylenes, 2003, p. 103–14. https://doi.org/10.1016/S1566-1369(03)80087-0.

[39] Contino M, Andena L, Rink M, Marra G, Resta S. Time-temperature equivalence in environmental stress cracking of high-density polyethylene. Eng Fract Mech 2018;203:32–43. https://doi.org/10.1016/j.engfracmech.2018.04.034.

[40] Andena L, Castellani L, Castiglioni A, Mendogni A, Rink M, Sacchetti F. Determination of environmental stress cracking resistance of polymers: Effects of loading history and testing configuration. Eng Fract Mech 2013;101:33–46. https://doi.org/10.1016/j.engfracmech.2012.09.004.

[41] Contino M, Andena L, Rink M, Colombo A, Marra G. Fracture of high-density polyethylene used for bleach bottles. Procedia Structural Integrity, vol. 2, Elsevier B.V.; 2016, p. 213–20. https://doi.org/10.1016/j.prostr.2016.06.028.

[42] Belcher JL, Brown HR. Crack branching and arrest in environmental cracking of polyethylene. J Mater Sci 1986;21:717–24. https://doi.org/10.1007/BF01145546.

[43] Tonyali K, Brown HR. On the applicability of linear elastic fracture mechanics to environmental stress cracking of low-density polyethylene. J Mater Sci 1986;21:3116–24. https://doi.org/10.1007/BF00553345.

[44] Tonyali K, Rogers CE, Brown HR. Stress-cracking of polyethylene in organic liquids. Polymer (Guildf) 1987;28:1472–7. https://doi.org/10.1016/0032-3861(87)90344-2.

[45] Tonyali K, Brown HR. Effects of detergent concentration and ethylene oxide chain length of the detergent molecule on stress-cracking of low-density polyethylene. J Mater Sci 1987;22:3287–92. https://doi.org/10.1007/BF01161193.

[46] Kamaludin MA, Patel Y, Williams JG, Blackman BRK. A fracture mechanics approach to characterising the environmental stress cracking behaviour of thermoplastics. Theoretical and Applied Fracture Mechanics 2017;92:373–80. https://doi.org/10.1016/j.tafmec.2017.06.005.

[47] Kamaludin MA, Patel Y, Blackman BRK, Williams JG. Fracture mechanics testing for environmental stress cracking in thermoplastics. Procedia Structural Integrity, vol. 2, Elsevier B.V.; 2016, p. 227–34. https://doi.org/10.1016/j.prostr.2016.06.030.

[48] Contino M, Andena L, La Valle V, Rink M, Marra G, Resta S. A comparison between K and G approaches for a viscoelastic material: the case of environmental stress cracking of HDPE. Mech Time Depend Mater 2020;24:381–94. https://doi.org/10.1007/s11043-019-09426-z.

[49] Bradley W, Cantwell WJ, Kausch HH. Viscoelastic Creep Crack Growth: A Review of Fracture Mechanical Analyses. Mech Time Depend Mater 1997;1:241–68. https://doi.org/10.1023/A:1009766516429.

[50] Stern A, Asanger F, Lang RW. Creep crack growth testing of plastics—II. data acquisition, data reduction and experimental results. Polym Test 1998;17:423–41. https://doi.org/10.1016/S0142-9418(97)00068-8.

[51] Cazenave J, Sixou B, Seguela R. Structural approaches of polyethylene environmental stress-crack resistance. Oil and Gas Science and Technology 2006;61:735–42. https://doi.org/10.2516/ogst:2006011.

[52] Friedrich K. Crazes and shear bands in semi-crystalline thermoplastics. In: Kausch HH, editor. Crazing in Polymers, Vol. 1, Advances in Polymer Science, vol. 52–53, Berlin, Heidelberg: Springer; 1983, p. 225–73. https://doi.org/10.1007/BFb0024054.

[53] Narisawa I, Ishikawa M. Crazing in Semicrystalline Thermoplastics. In: Kausch HH, editor. Crazing in Polymers Vol. 2, vol. 91–92, Springer; 1990, p. 353–91. https://doi.org/10.1007/BFb0018017.

[54] Isaksen RA, Newman S, Clark RJ. Mechanism of environmental stress cracking in linear polyethylene. J Appl Polym Sci 1963;7:515–31. https://doi.org/10.1002/app.1963.070070210.

[55] Bandyopadhyay S, Brown HR. Evidence of interlamellar failure in environmental stress cracking of polyethylene. J Mater Sci 1977;12:2131–4. https://doi.org/10.1007/BF00561990.

[56] Keith HD, Padden FJ, Vadimsky RG. Intercrystalline links in polyethylene crystallized from the melt. Journal of Polymer Science Part A-2: Polymer Physics 1966;4:267–81. https://doi.org/10.1002/pol.1966.160040208.

[57] Lu X, Ishikawa N, Brown N. The critical molecular weight for resisting slow crack growth in a polyethylene. J Polym Sci B Polym Phys 1996;34:1809–13. https://doi.org/https://doi.org/10.1002/(SICI)1099-0488(19960730)34:10<1809::AID-POLB12>3.0.CO;2-F.

[58] Huang Y-L, Brown N. The effect of molecular weight on slow crack growth in linear polyethylene homopolymers. J Mater Sci 1988;23:3648–55. https://doi.org/10.1007/BF00540508.

[59] Seguela R. Critical review of the molecular topology of semicrystalline polymers: The origin and assessment of intercrystalline tie molecules and chain entanglements. J Polym Sci B Polym Phys 2005;43:1729–48. https://doi.org/10.1002/polb.20414.

[60] Lustiger A, Markham RL. Importance of tie molecules in preventing polyethylene fracture under long-term loading conditions. Polymer (Guildf) 1983;24:1647–54. https://doi.org/10.1016/0032-3861(83)90187-8.

[61] Lustiger A. Environmental Stress Cracking: The Phenomenon and Its Utility. In: Brostow W, Corneliussen RD, editors. Failure of Plastics, Munich; New York: Hanser Publishers; 1986, p. 305–29.

[62] Plummer CJG, Goldberg A, Ghanem A. Micromechanisms of slow crack growth in polyethylene under constant tensile loading. Polymer (Guildf) 2001;42:9551–64. https://doi.org/10.1016/S0032-3861(01)00476-1.

[63] Huang Y, Brown N. Dependence of slow crack growth in polyethylene on butyl branch density: Morphology and theory. J Polym Sci B Polym Phys 1991;29:129–37. https://doi.org/10.1002/polb.1991.090290116.

[64] McDermott AG, Deslauriers PJ, Fodor JS, Jones RL, Snyder CR. Measuring Tie Chains and Trapped Entanglements in Semicrystalline Polymers †. Macromolecules 2020;53:5614–26. https://doi.org/10.1021/acs.macromol.0c00132.

[65] Fodor JS, DesLauriers PJ, Lamborn MJ, Hamim SU. Further investigation of the relationship between polymer structure and HDPE post yield properties. Polymer (Guildf) 2019;180. https://doi.org/10.1016/j.polymer.2019.121730.

[66] DesLauriers PJ, Lamborn MJ, Fodor JS. Correlating polyethylene microstructure to stress cracking; correlations to post yield tensile tests. Polymer (Guildf) 2018;153:422–9. https://doi.org/10.1016/j.polymer.2018.08.023.

[67] Deslauriers PJ, Rohlfing DC. Estimating slow crack growth performance of polyethylene resins from primary structures such as molecular weight and short chain branching. Macromol Symp, vol. 282, 2009, p. 136–49. https://doi.org/10.1002/masy.200950814.

[68] Patel RM, Sehanobish K, Jain P, Chum SP, Knight GW. Theoretical prediction of tie-chain concentration and its characterization using postyield response. J Appl Polym Sci 1996;60:749–58. https://doi.org/10.1002/(SICI)1097-4628(19960502)60:5<749::AID-APP14>3.0.CO;2-U.

[69] Yeh JT, Runt J. Fatigue crack propagation in high-density polyethylene. J Polym Sci B Polym Phys 1991;29:371–88. https://doi.org/10.1002/polb.1991.090290313.

[70] Fischer EW. Studies of structure and dynamics of solid polymers by elastic and inelastic neutron scattering. Pure and Applied Chemistry 1978;50:1319–41. https://doi.org/10.1351/pac197850111319.

[71] Brown N, Ward IM. The influence of morphology and molecular weight on ductile-brittle transitions in linear polyethylene. J Mater Sci 1983;18:1405–20. https://doi.org/10.1007/BF01111960.

[72] Lustiger A, Ishikawa N. An analytical technique for measuring relative tie-molecule concentration in polyethylene. J Polym Sci B Polym Phys 1991;29:1047–55. https://doi.org/10.1002/polb.1991.090290902.

[73] Bartczak Z. Evaluation of effective density of the molecular network and concentration of the stress transmitters in amorphous layers of semicrystalline polyethylene. Polym Test 2018;68:261–9. https://doi.org/10.1016/j.polymertesting.2018.04.027.

[74] Litvinov V, Deblieck R, Clair C, Van Den Fonteyne W, Lallam A, Kleppinger R, et al. Molecular Structure, Phase Composition, Melting Behavior, and Chain Entanglements in the Amorphous Phase of High-Density Polyethylenes. Macromolecules 2020;53:5418–33. https://doi.org/10.1021/acs.macromol.0c00956.

[75] Fawaz J, Deveci S, Mittal V. Molecular and morphological studies to understand slow crack growth (SCG) of polyethylene. Colloid Polym Sci 2016;294:1269–80. https://doi.org/10.1007/s00396-016-3888-5.

[76] Sardashti P, Stewart KME, Polak M, Tzoganakis C, Penlidis A. Operational maps between molecular properties and environmental stress cracking resistance. J Appl Polym Sci 2019;136. https://doi.org/10.1002/app.47006.

[77] Deveci S, Kaliappan SK, Fawaz J, Gadgoli U, Das B. Sensitivity of post yield axial deformation properties of high-density ethylene/α-olefin copolymers in relation to molecular structure and slow crack growth resistance. Polym Test 2018;72:285–97. https://doi.org/10.1016/j.polymertesting.2018.10.032.

[78] Lu X, Brown N. Effect of thermal history on the initiation of slow crack growth in linear polyethylene. Polymer (Guildf) 1987;28:1505–11. https://doi.org/10.1016/0032-3861(87)90350-8.

[79] Mandelkern L, Alamo RG, Kennedy MA. The interphase thickness of linear polyethylene. Macromolecules 1990;23:4721–3. https://doi.org/10.1021/ma00223a034.

[80] Bubeck RA, Baker HM. The influence of branch length on the deformation and microstructure of polyethylene. Polymer (Guildf) 1982;23:1680–4. https://doi.org/10.1016/0032-3861(82)90193-8.

[81] García RA, Carrero A, Martín C, Domínguez C. Effects of the structural components on slow crack growth process in polyethylene blends. Composition intervals prediction for pipe applications. J Appl Polym Sci 2011;121:3269–76. https://doi.org/10.1002/app.33911.

[82] Huang Y, Brown N. The dependence of butyl branch density on slow crack growth in polyethylene: Kinetics. J Polym Sci B Polym Phys 1990;28:2007–21. https://doi.org/10.1002/polb.1990.090281110.

[83] He X, Zha X, Zhu X, Qi X, Liu B. Effect of short chain branches distribution on fracture behavior of polyethylene pipe resins. Polym Test 2018;68:219–28. https://doi.org/10.1016/j.polymertesting.2018.04.017.

[84] Cheng JJ, Polak MA, Penlidis A. Influence of micromolecular structure on environmental stress cracking resistance of high density polyethylene. Tunnelling and Underground Space Technology 2011;26:582–93. https://doi.org/10.1016/j.tust.2011.02.003.

[85] Krishnaswamy RK, Yang Q, Fernandez-Ballester L, Kornfield JA. Effect of the distribution of short-chain branches on crystallization kinetics and mechanical properties of high-density polyethylene. Macromolecules 2008;41:1693–704. https://doi.org/10.1021/ma070454h.

[86] Hosoda S, Uemura A. Effect of the Structural Distribution on the Mechanical Properties of Linear Low-Density Polyethylenes. Polym J 1992;24:939–49. https://doi.org/10.1295/polymj.24.939.

[87] Gupta P, Wilkes GL, Sukhadia AM, Krishnaswamy RK, Lamborn MJ, Wharry SM, et al. Does the length of the short chain branch affect the mechanical properties of linear low density polyethylenes? An investigation based on films of copolymers of ethylene/1-butene, ethylene/1-hexene and ethylene/1-octene synthesized by a single site metallocene catalyst. Polymer (Guildf) 2005;46:8819–37. https://doi.org/10.1016/j.polymer.2005.05.137.

[88] Yeh JT, Chen J, Hong H. Environmental stress cracking behavior of short-chain branch polyethylenes in Igepal solution under a constant load. J Appl Polym Sci 1994;54:2171–86. https://doi.org/10.1002/app.1994.070541320.

[89] Yeh JT, Chen CY, Hong HS. Static fatigue behaviour of linear low-density polyethylenes. J Mater Sci 1994;29:4104–12. https://doi.org/10.1007/BF00355978.

[90] Hosoda S, Nomura H, Gotoh Y, Kihara H. Degree of branch inclusion into the lamellar crystal for various ethylene/α-olefin copolymers. Polymer (Guildf) 1990;31:1999–2005. https://doi.org/10.1016/0032-3861(90)90030-3.

[91] Doran M, Choi P. Molecular dynamics studies of the effects of branching characteristics on the crystalline structure of polyethylene. J Chem Phys 2001;115:2827–30. https://doi.org/10.1063/1.1386907.

[92] Zhang X, Li Z, Yang H, Sun C-C. Molecular Dynamics Simulations on Crystallization of Polyethylene Copolymer with Precisely Controlled Branching. Macromolecules 2004;37:7393–400. https://doi.org/10.1021/ma030010v.

[93] Sanmartín S, Ramos J, Martínez-Salazar J. Following the Crystallization Process of Polyethylene Single Chain by Molecular Dynamics: The Role of Lateral Chain Defects. Macromol Symp 2012;312:97–107. https://doi.org/10.1002/masy.201100006.

[94] Formenti G. Environmental Stress Cracking of Polyethylenes. MSc Thesis; 2019.

[95] International Organization for Standardization. Rubber, vulcanized or thermoplastic – Determination of tensile stress-strain properties 2024.

[96] Ferry JD. Viscoelastic properties of polymers. J. Wiley; 1980.

[97] Tschoegl NW. The Phenomenological Theory of Linear Viscoelastic Behavior. Springer Nature; 1989. https://doi.org/10.1007/978-3-642-73602-5.

[98] Christensen RM. Theory of viscoelasticity. Dover Publications; 2003.

[99] Brinson HF, Brinson LC, Service S (Online. Polymer Engineering Science and Viscoelasticity : An Introduction. Springer Us; 2010.

[100] Machida K. JIG evaluation and effective thickness of thin specimens with and without side-grooves. International Journal of Pressure Vessels and Piping 1997;71:181–8. https://doi.org/10.1016/S0308-0161(96)00067-1.

[101] Stam G. The stress intensity factor for grooved DCB specimens loaded by splitting forces. Int J Fract 1996;76:341–54.

[102] Castiglioni A, Andena L, Castellani L, Mendogni A, Rink M, Sacchetti F, et al. Environmental crack initiation and propagation in polyethylene under different loading conditions, 2012.

[103] Frassine R, Rink M, Leggio A, Pavan A. Experimental analysis of viscoelastic criteria for crack initiation and growth in polymers. vol. 81. Kluwer Academic Publishers; 1996. https://doi.org/https://doi.org/10.1007/BF00020755.

[104] Rooke DP, Cartwright DJ. Compendium of Stress Intensity Factors. Uxbridge: The Hillingdon Press; 1976.

[105] Chudnovsky A. Slow crack growth, its modeling and crack-layer approach: A review. Int J Eng Sci 2014;83:6–41. https://doi.org/10.1016/j.ijengsci.2014.05.015.

[106] Lu X, Qian R, Brown N. Discontinuous crack growth in polyethylene under a constant load. J Mater Sci 1991;26:917–24. https://doi.org/10.1007/BF00576768.

[107] Frassine R, Rink M, Pavan A. Discontinuous creep crack-growth in polyethylene. Plastic Pipes Conference Association 1995:257–65.

[108] Séguéla R. On the Natural Draw Ratio of Semi-Crystalline Polymers: Review of the Mechanical, Physical and Molecular Aspects. Macromol Mater Eng 2007;292:235–44. https://doi.org/10.1002/mame.200600389.

[109] J. G. Williams, G. P. Marshall. Environmental crack and craze growth phenomena in polymers. Proceedings of the Royal Society of London A Mathematical and Physical Sciences 1975;342:55–77. https://doi.org/10.1098/rspa.1975.0012.

[110] Anderson TL. Fracture Mechanics: Fundamentals and Applications. 3rd ed. Boca Raton, FL: CRC Press; 2004.

[111] Timoshenko S, Goodier JN. Theory of Elasticity. 2nd ed. New York: McGraw-Hill Book Company; 1951.

[112] Öchsner A. Classical Beam Theories of Structural Mechanics. Cham: Springer; 2021.